Title: NBR1-mediated selective autophagy of ARF7 modulates root branching

Running title: Autophagy modulates root branching

Ebstrup E[1+], Ansbøl J[1+], Paez-Garcia A[2], Culp H[1], Chevalier J[1], Clemmens P[1], Coll NS[3,4], Moreno-Risueno M A[2], Rodriguez E[1*]

[1]Department of Biology, University of Copenhagen, 2200 Copenhagen N, Denmark.

[2]Centro de Biotecnología y Genómica de Plantas (Universidad Politécnica de Madrid (UPM) – Instituto Nacional de Investigación y Tecnología Agraria y Alimentaria- CSIC (INIA/CSIC)). Campus de Montegancedo, Pozuelo de Alarcón, 28223, Madrid, Spain

[3]Centre for Research in Agricultural Genomics (CRAG), CSIC-IRTA-UAB-UB, Bellaterra 08193, Spain

[4]Consejo Superior de Investigaciones Científicas (CSIC), Barcelona 08001, Spain

[+]These authors contributed equally to this work.

*Correspondence to: Eleazar.rodriguez@bio.ku.dk

Abstract

Auxin dictates root architecture via the Auxin Response Factor (ARF) family of transcription factors, which control lateral root (LR) formation. In *Arabidopsis*, ARF7 regulates the specification of prebranch sites (PBS) generating LRs through gene expression oscillations and plays a pivotal role during LR initiation. Despite the importance of ARF7 in this process, there is a surprising lack of knowledge about how ARF7 turnover is regulated and how this impacts root architecture. Here, we show that ARF7 accumulates in autophagy mutants and is degraded through NBR1-dependent selective autophagy. We demonstrate that the previously reported rhythmic changes to ARF7 abundance in roots are modulated via autophagy and might occur in other tissues. Additionally, we prove that the level of co-localization between ARF7 and autophagy markers oscillates and can be modulated by auxin to trigger ARF7 turnover. Furthermore, we observed that autophagy impairment prevents ARF7 oscillation and reduces both PBS establishment and LR formation. In conclusion we report a novel role for autophagy during development, namely by enacting auxin-induced selective degradation of ARF7 to optimize periodic root branching.

Introduction

The plant root system plays a fundamental role as a point of contact with the plant surroundings and allows adaptation to multiple stresses. Contrary to primary roots, lateral root (LR) development is post embryonic, which allows LR architecture to be influenced by growth conditions (Lv *et al*, 2021). As LR growth is modular, perception of the correct developmental conditions enables the repetition of LR modules along the primary root, maximizing the root's surface area. LRs originate from a cell type called pericycle which surrounds the vasculature, and occurs sequentially in 4 steps: positioning, initiation, outgrowth, and emergence. During the positioning step, the plant ensures the spatiotemporal distribution, priming and activation of LR founder cells (LRFC) (Du & Scheres, 2018). LR spacing is controlled by the root clock which dictates oscillatory gene expression and cycles every 4-6 hours (Moreno-Risueño *et al*, 2010). This oscillatory clock is regulated, among others, by the phytohormone auxin and can be characterized through monitoring of reporter marker expression driven by DR5, a synthetic promoter containing tandem repeats of an auxin responsive TGTCTC element (Ulmasov *et al*, 1997). DR5 expression analyses led to the definition of 2 contrasting oscillation phases: in-phase (concurrent with DR5 maximum signal) and anti-phase (DR5 minimum signal) which reciprocally repress each other (Moreno-Risueño *et al*, 2010). One of the genes displaying anti-phase expression is AUXIN RESPONSIVE FACTOR 7 (*ARF7*), a key transcription factor (TF) which, among others, regulates different steps of LR formation (Okushima *et al*, 2007). Importantly, analysis of *ARF7* loss of function mutant (Moreno-Risueño *et al*, 2010; Perianez-Rodriguez *et al*, 2021) indicates that ARF7 is part of the core oscillator of the root clock and that this TF's oscillation is essential for the correct establishment of LR prebranch sites (PBS).

While positioning and initiation are broadly regulated by different mechanisms (Wachsman *et al*, 2020; Perez-Garcia *et al* 2022), ARF7 and its 2 direct targets LATERAL ORGAN BOUNDARIES DOMAIN 16 (LBD16) and LBD33 are among the few genes that participate in both processes (Moreno-Risueño *et al*, 2010) which attests to ARF7 pivotal role in organizing root architecture. During the initiation step, which follows PBS specification, the auxin signalling node IAA14-ARF7-ARF19 controls LBD16 activation in the LRFC, which is necessary to achieve asymmetry and initiate cell division (Goh *et al*, 2019). In addition to the importance of *ARF7* transcriptional oscillation for LR formation, it has also been shown that the subcellular localization of ARF7 is important for its function: nuclear localization correlates with auxin responsive tissues while in less responsive areas, activating ARFs concentrate to form cytoplasmic condensates with liquid-like and solid-like proprieties (Powers *et al*, 2019). This body of evidence demonstrate the regulatory complexity coordinating ARFs-dependent responses, encompassing an intricate web of processes

which tightly regulate ARFs levels and compartmentalization. Yet surprisingly, little is known about how ARF7 degradation is managed and how does it impact the cellular decision making behind LR formation.

Macroautophagy (herein autophagy) is an evolutionary conserved catabolic process which partakes in cellular recycling of macromolecules and organelles (Levine & Klionsky, 2004). Autophagy is characterized by the formation of an isolation membrane enclosing a portion of cytoplasm to form a double-membraned vesicle termed the autophagosome. Originally characterized during starvation stress, autophagy was viewed as a bulk degradation process due to the observation of what seemed to be an indiscriminate engulfment of portions of the cytoplasm. Further studies unveiled the existence of several selective cargo adaptors which allow for targeted degradation of cellular constituents (*e.g.,* Svenning *et al*, 2011; Nolan *et al*, 2017; Stephani *et al*, 2020; Wu *et al*, 2021), meaning that autophagy can be highly selective and participate in targeted remodelling of the cell. Perhaps one of the most characterized cargo receptors in plants is NEIGHBOUR OF BRCA1 (NBR1, Svenning *et al*, 2011), a hybrid of mammalian NBR1 and p62, which possess a PB1 domain necessary for homopolymerization and biomolecular condensate formation, and an UBA domain for ubiquitin binding. It is through the latter that NBR1 binds ubiquitinated cargo, which is then targeted for autophagic degradation via NBR1 interaction with the autophagosome decorating proteins ATG8s (*e.g.,* Zhou *et al*, 2013, 2014; Hafrén *et al*, 2017; Ji *et al*, 2020; Tarnowski *et al*, 2020). The ability to function selectively allows autophagy to participate in a variety of stress responses, namely by promoting the cellular reprogramming necessary to enact appropriated responses (Rodriguez *et al*, 2020). Consistent with this homeostatic role, autophagic deficiency has been shown to cause diverse developmental defects in animals; interference with core autophagic machinery component often causes lethality during early developmental stages, severe developmental defects, and shortened life span (*e.g.,* Scott *et al*, 2004; Liu *et al*, 2015; Yoshii *et al*, 2016). In contrast, plants are able to tolerate disruption of autophagy activity without major penalties: autophagy deficient mutants display growth phenotypes such as decrease in biomass, reduced inflorescence numbers and premature senescence (Bassham *et al*, 2006), but importantly, they are able to complete their life cycle and generate fertile progeny. However, these mild phenotypes displayed by plant *atg* mutants become more apparent under stress, as can be attested by the many publications linking autophagy with stress responses (Liu *et al*, 2009; Hofius *et al*, 2009; Vanhee *et al*, 2011; Zhou *et al*, 2013b; Coll *et al*, 2014; Munch *et al*, 2014; Chen *et al*, 2015; Nolan *et al*, 2017; Sedaghatmehr *et al*, 2019; Rodriguez *et al*, 2020). For instance, under nutrient starvation, autophagy has been shown to help sustain primary root growth and LR formation (Deb *et al*, 2014; Huang *et al*, 2019). However, if and how autophagy impacts root

architecture under normal developmental conditions is currently unknown and warrants close examination.

In this work, we explored how autophagy impacts ARF7-dependent responses during LR formation. By using a combination of cell imaging, biochemical, genetics, molecular biology, and proteomics approaches, we demonstrate that ARF7 turnover is processed via NBR1-mediated selective autophagy. Importantly, we demonstrate that ARF7 abundance, which rhythmically oscillates, requires autophagy and subsequently autophagy alters the oscillatory patterning. Moreover, we show that a short auxin treatment is sufficient to trigger ARF7 condensation and co-localization with ATG8a, thought this mainly occurs in the oscillation and maturation zones. Consistent with this, autophagy deficiency reduces PBS establishment and LR formation. With these findings, we reveal an important regulatory role for selective autophagy during auxin responses through the turnover of the crucial auxin signalling regulator ARF7 and consequent fine-tuning of root architecture.

Results

Autophagy modulates ARFs *turnover*

We have recently reported that autophagy participates in stem cell reprogramming and differentiation in the distantly related species *Physcometrilla. patens* and *Arabidopsis* (Rodriguez *et al*, 2020; Kanne *et al*, 2021). Because *Arabidopsis* stem cell hormonal reprogramming executes a developmental program similar to LR initiation (Sugimoto *et al*, 2010), we wondered if key regulators of these processes might be modulated via autophagy. As seen in Fig 1, ARF7 accumulates in different autophagy mutants (*atg*) and in the knock-out mutant (KO) of the autophagic cargo adaptor NBR1 (Fig 1A), when compared to Col-0. To address if the proteasome also contributes to ARF7 proteostasis, we treated seedlings of those genotypes with the proteasome inhibitor MG132 (Fig 1A). Col-0 samples treated with MG132 showed ARF7 accumulation to levels comparable with those of untreated *atg* mutants. Moreover, simultaneous inhibition of both degradation pathways (MG132 treatment in *atg* mutants) led to further accumulation of ARF7, which indicate that ARF7 degradation is dependent on autophagy and the proteasome and is in agreement with previous data showing proteasomal degradation of ARF7 (Jing *et al*, 2022). To rule out that elevated transcript levels in *atg* mutants could underscore ARF7 accumulation in those lines, we performed qPCR and observed that *ARF7* relative expression was not statistically significant among lines tested (Fig 1B).

To further support our claim that autophagy modulates ARF7 turnover, we introduced the translational reporter *pARF7::gARF7-Venus* herein called *ARF7-Venus* (Orosa-Puente *et al*, 2018) into *atg2-1* background. We then quantified ARF7-Venus levels by western blot analyses of protein extracts from *ARF7-Venus* and *ARF7-Venus x atg2-1*¸ detecting significantly higher levels of ARF7-Venus when autophagy is dysfunctional (Fig 1C). Using the same lines, we also analysed ARF7-Venus subcellular fluorescence intensity in the root meristematic and maturation zones by confocal microscopy (Fig 1 D-I). In agreement with the western blot data, we detected significantly higher ARF7-Venus fluorescence intensity in the *atg2-1* background for all tissues and subcellular localization except for the meristem's nuclei (Fig1 I). Because ARF7 often works together with ARF19 during regulation of root architecture, we also enquired about a role for autophagy during ARF19 turnover. Western blot probing of *pARF19::ARF19-GFP* expressed in an *ARF7* and *ARF19* double loss of function mutant (*nph4-1 arf19-1)* (Okushima *et al*, 2007) treated with or without the vacuolar protease inhibitors Pepstatin A and E-64D for 24h revealed substantial accumulation of ARF19-GFP when vacuolar proteases were inhibited (Fig EV1). Together, our results indicate that autophagy participates in the turnover of these essential developmental regulators.

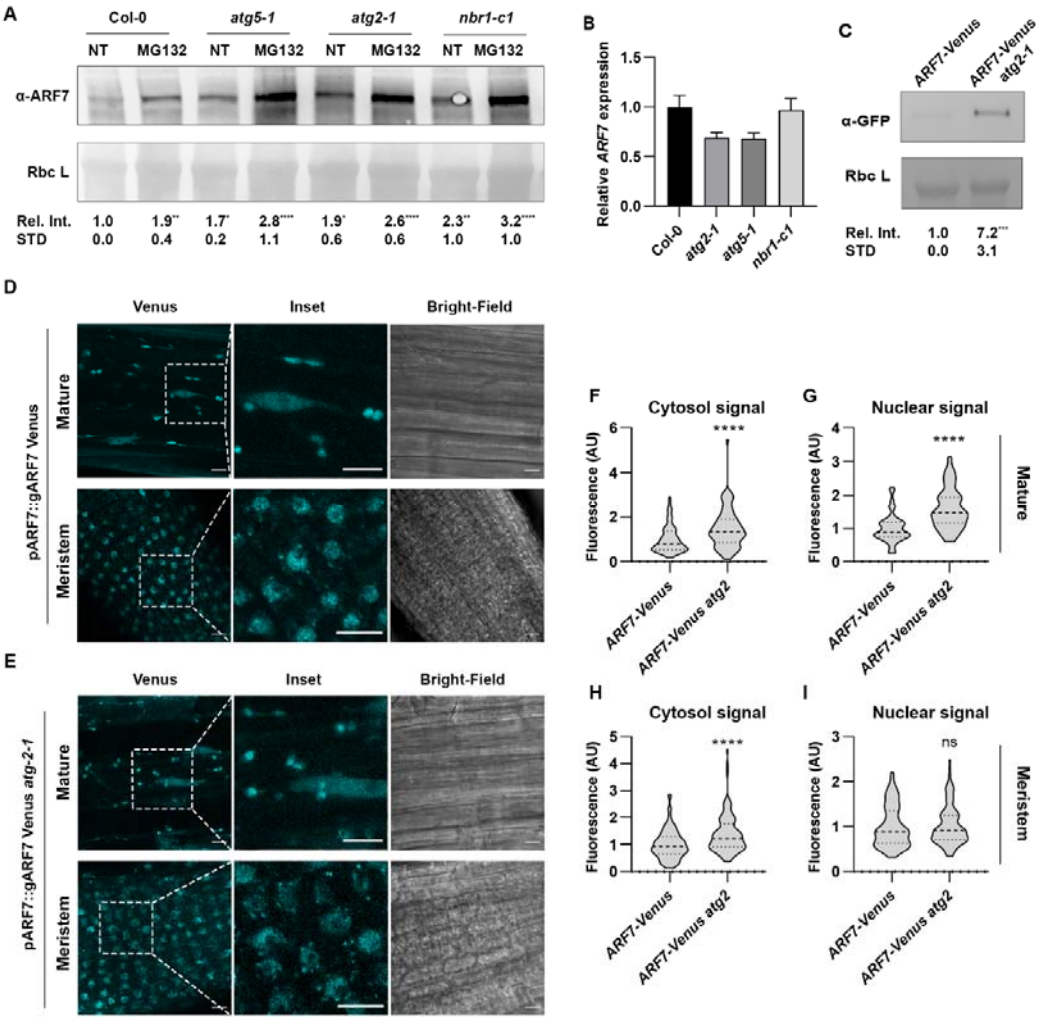

Figure 1*:* ARF7 is degraded via autophagy. **A**) ARF7 western blots of protein extracts from Col-0, *atg5-1*, *atg2-1* and *nbr1-c1* with or without addition of the proteasome inhibitor MG132. **B**) *ARF7* relative expression in given genotypes. *ARF7* expression was normalized to *ACTIN2,* and values are relative to Col-0 (set to 1). The experiment was repeated 3 times (biological replicates) with similar results. **C**) GFP western blot of protein extracts from Col-0 or *atg2-1* expressing *ARF7-Venus.* Values below each band represent the relative intensity ratio between ARF7 (**A**) or ARF7-Venus (**C**) and RuBisCO large subunit (Rbc L) as stained with Ponceau S used as loading control. Ratios were normalized to untreated Col-0 NT (MS+ solvent) which was arbitrarily set to 1. Values provided are the average and SD of 5 **(A)** or 7 **(C)** biological replicates, asterisk depict statistical significance from Col-0 NT according to a Holm-Sidak test **(A)** or two-tailed t-test **(C)** (* 0.05; ** 0.01; **** 0.0001). **D-E**) Confocal images of root maturation zone (top panel) and meristematic zone (bottom panel) in Col-0 (**D**) or *atg2-1* (**E**) expressing *ARF7-Venus*. (**F-I**) Fluorescence intensity quantification of ARF7-Venus subcellular localization in given lines. The values presented for ARF7-Venus fluorescence intensity in *atg2-1* background in the maturation zone (**F-G**) or meristematic zone (**H-I**) were normalized to the values in Col-0 background (which was set to 1). The outline of the violin plots represents the probability of the kernel density. Dotted lines represent interquartile ranges (IQR), with the thick horizontal line representing the median; whiskers extend to the highest and lowest data point. Results were obtained from three independent experiments with at least 11 plants per condition being analysed in total. At least 40 nuclei and cytoplasmic regions were measured per genotype/tissue. Asterisks mark statistical significance to NT according to a Mann-Whitney U-test (****P < 0.0001).

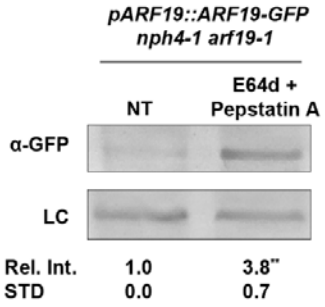

Fig EV1*:* Autophagy inhibition promotes ARF19 accumulation. GFP western blot of 14-day-old *pARF19::ARF19-GFP/nph4-1 arf19-1* seedlings grown in MS or MS supplemented with vacuolar protease inhibitors E-64D and Pepstatin A for 24h. Values below each band represent the ratio between ARF19-GFP and the loading control (LC) normalized to NT (MS+ solvent), which was set to 1. Image is representative of 3 biological replicates; asterisk depict statistical significance from NT according to a Man—Whitney U-test (P≤0.01)

ARF7 *interacts with* NBR1 *and* ATG8a *in planta*

To further substantiate our claim that autophagy participates in the targeted degradation of ARF7 we performed protein-protein interaction studies. For this purpose, we used stable transgenic lines expressing ARF7-Venus and performed coimmunoprecipitation (Co-IP) experiments using anti-NBR1 and anti-ATG8a antibodies. The experiment revealed that NBR1 (Fig 2A) but not GOLGI TRANSPORT 1 (GOT1) YFP, co-immunoprecipitated with ARF7-Venus; this is supported by an observable enrichment of ATG8a in the same conditions (Fig 2B). Moreover, a web-based analysis identified several potential ATG8-interaction motifs (AIM) in ARF7(Jacomin *et al*, 2016), supporting our findings. As a cautionary note, we were unable to detect ARF7-Venus in the input of both Co-IPs which can likely be explained by the fact that ARF7-Venus is under the control of its native promoter and thus lowly expressed and/or differences between the protein extraction buffers used. We also performed multi-colour Bimolecular fluorescence complementation (mcBiFC) analysis with a system allowing simultaneous interaction studies of several proteins (Gehl *et al*, 2009) to transiently express Venus^{N}-ARF7 with SCFP^{N}-ATG8a and either SCFP^{C}-NBR1 or SCFP^{C}-TSPO, (TRYPTOPHAN-RICH SENSORY PROTEIN, an autophagic cargo adaptor for aquaporins, Hachez *et al*, 2014) in *Nicotiana benthamiana* leaves. As expected, SCFP^{C}-NBR1 and SCFP^{N}-ATG8a were able to reconstitute CFP to produce distinct fluorescence signal localized in the nuclei and cytoplasm (Fig 2C). Moreover, Venus^{N}-ARF7 and SCFP^{C}-NBR1 produced GFP signal, which was localized to the cytoplasm and nuclei, in many instances co-localizing with NBR1-ATG8a CFP signal (Fig 2C). In contrast, SCFP^{C}-TSPO did not produce GFP signal when co-expressed with Venus^{N}-ARF7. In combination, these results indicate that ARF7 interacts with autophagic components and cumulative with

data from Fig 1, indicate that this TF is degraded, in part, via NBR1-mediated selective autophagy.

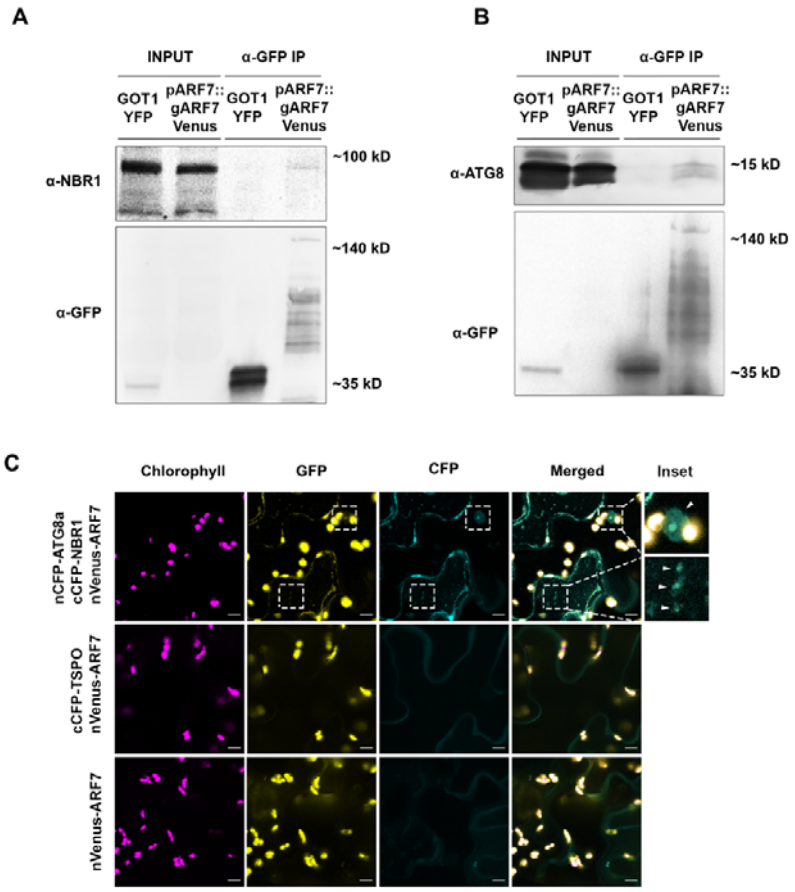

Figure 2 ARF7 associates with the autophagic components NBR1 and ATG8a. **A, B)** ARF7 and ATG8/NBR1 association was tested using a coimmunoprecipitation (Co-IP) assay. Protein extracted from *Arabidopsis* lines expressing *pARF7::gARF7-Venus* or free *YFP* were immunoprecipitated with anti-GFP antibody and subsequently probed with antibodies raised against NBR1 or ATG8a. Apparent molecular weights: ARF7-Venus ~150 kDa; GOT1-GFP ~45 kDa; NBR1 ~100 kDa; ATG8 ~15 kDa; **C**) Bimolecular fluorescence complementation experiments showed oligomerization of ARF7, NBR1 and ATG8a in *N. Benthamiana*. Images were taken 48 hpi. cCFP-TSPO was used as control. Insets display close-ups of examples of reconstitution of GFP and CFP signal, which are also indicated by arrows. Etched boxes in GFP and CFP channels indicate the place of the insets in those channels. Scale bar: 10 µM

ARF7 co-localizes with autophagosomes following and varies with time.

Having established that autophagy regulates ARF7 abundance, it would be expected that this TF co-localized with autophagosome-like structures. To assess this, we crossed ARF7-Venus to mCherry-ATG8a and mCherry-NBR1 reporter lines (Svenning *et al*, 2011) and used this for live cell imaging. As expected, both autophagy-related proteins localized to

cytoplasmic foci, in many instances co-localizing with ARF7-Venus (Fig 3A). Moreover, mCherry-ATG8a also co-localized with ARF7-Venus in the nucleus (Fig 3A). It should be noted that the co-localization of these autophagic proteins with ARF7 in cytoplasmic foci is mainly observable in mature tissue (Fig 3A & B); in younger meristematic tissue ARF7 primarily localizes in the nucleus although some instances of cytoplasmic co-localization are also observable (Fig 3A, white arrows). These findings are in agreement with previous reports demonstrating that ARF7 partitioning is dependent on the developmental stage of the tissue (Orosa-Puente *et al*, 2018; Powers *et al*, 2019).

ARF7's nucleo-cytopartitioning has been ascribed to liquid-liquid phase separation (LLPS) (Powers *et al*, 2019); likewise, autophagosome formation sites and protein cargo triage (Kirkin *et al*, 2009; Zhang *et al*, 2009; Fujioka *et al*, 2020) are also dependent on LLPS. To address the nature of these cytoplasmic ARF7 & ATG8 foci, we incubated seedlings expressing mCherry-ATG8 and ARF7-Venus with the LLPS inhibitor 1,6-hexanediol (Wang *et al*, 2021; Xie *et al*, 2021) and tracked the stability of those foci over time. Most of the foci in which ARF7-Venus and mCherry-ATG8a co-localized were sensitive to 1,6-hexanediol treatment (Fig EV2), suggesting that these structures have liquid-like properties. Our data is both in agreement with findings for ARF7 (Powers *et al*, 2019) and studies in mammalians showing that NBR1 (and p62) is involved in condensate formation during autophagic degradation of substrates (Turco *et al*, 2021).

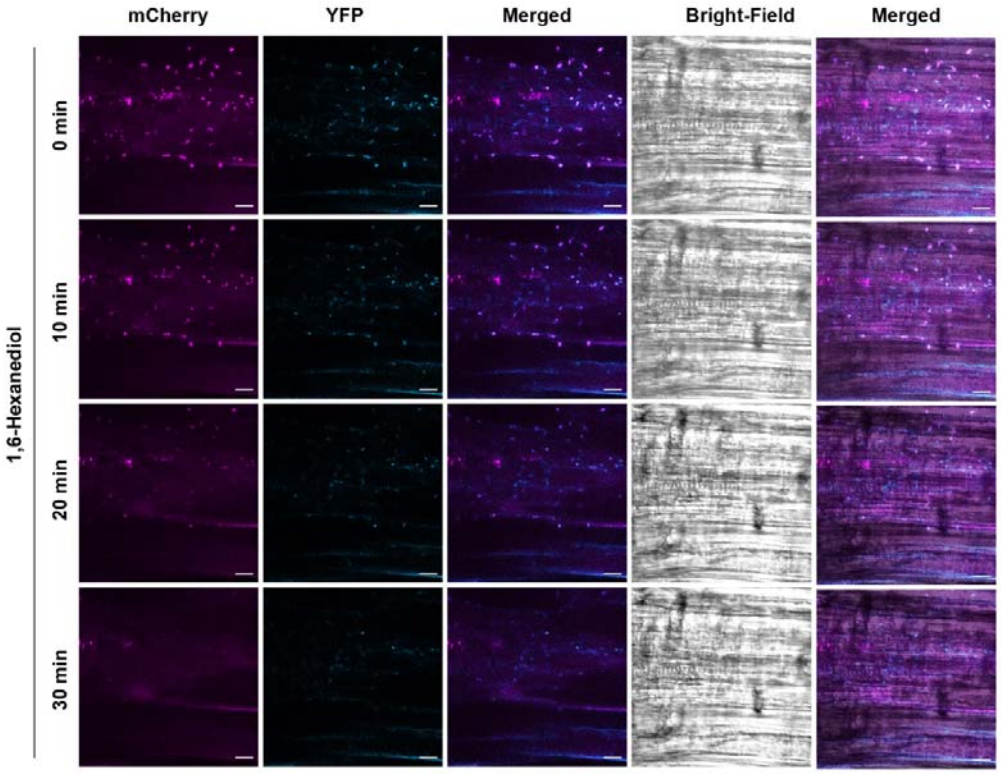

Figure EV2 ARF7 and ATG8 condensates have liquid properties. *pARF7::gARF7-Venus* x *mCherry ATG8a* plants were treated with the LLPS inhibitor 1,6-Hexanediol and imaged at given time points. Representative pictures were taken in the maturation zone of 10–14-day old *Arabidopsis* seedlings. Leftmost Merge column represent the merger of YFP and mCherry channels, while the rightmost also includes the T-PMT channel (Brightfield). Scale bar 10 µM.

Interestingly, during the course of our experiments we noticed that the co-localization of ARF7-Venus with mCherry-ATG8a varied with time, *i.e.,* there was a significant increase (45% to 85%, $P<0.05$) in ARF7 and ATG8a co-localization in the maturation zone when comparing seedlings during a period of approximately 6h. This is consistent with previous reports (Perianez-Rodriguez *et al*, 2021) showing that *ARF7* transcript levels follow periodic fluctuation in roots. Next, we incubated seedlings with vacuole protease inhibitors (Pepstatin A and E-64d) which led to a dramatic increase in ARF7-Venus co-localization with mCherry-ATG8a (Fig 3C & D). This both supports our findings with *ARF7-Venus* x *atg2-1* (Fig 1) as well as the proposition that ARF7 condensate formation can be linked to autophagic degradation. Altogether, our results suggest that ARF7 cytoplasmic localization might be part of a proteome remodelling strategy which is mediated, at least in part, via autophagy.

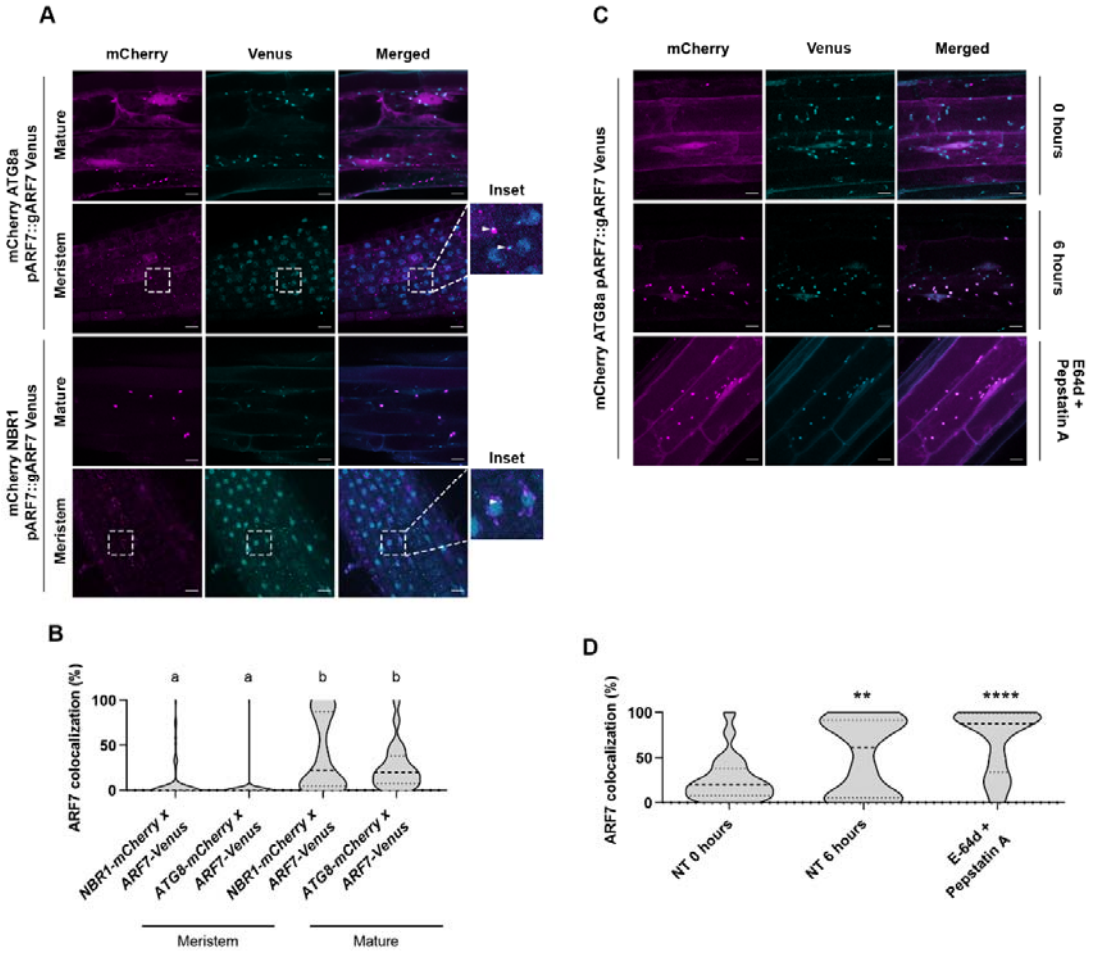

Figure 3 ARF7 co-localization with autophagosomes displays spatial and rhythmic variation. **A**) Co-localization of ARF7-Venus with mCherry-ATG8a (nuclei and/or cytoplasmic foci) or mCherry-NBR1 (cytoplasmic foci) in meristem or maturation zone. Pictures were taken in the respective root zone of 10–14-day old *Arabidopsis* seedlings. Scale bar 10 µM. Insets display close-ups of regions of the meristem, white arrow indicates instances of co-localization between mCherry-ATG8a (Top)/mCherry-NBR1(bottom) and ARF7-Venus foci. Etched boxes in mCherry and Venus channels indicate the place of the insets in those channels. **B**) Quantification of the co-localization of ARF7-Venus with mCherry-ATG8a or NBR1 under conditions depicted in **A)**; samples followed by the same letters are not statistically different (Dunn's test, P≤0.0001). **C)** ARF7-Venus co-localization with autophagosomes under selected treatments: No Treatment (NT, 0h or 6h), E-64d + Pepstatin A (vacuolar protease inhibitors. Scale bar 10 µM. **D)** Quantification of the co-localization of ARF7-Venus with mCherry-ATG8a under conditions depicted in **C)**. The outline of the violin plots represents the probability of the kernel density. Dotted lines represent interquartile ranges (IQR), with the thick horizontal line representing the median; whiskers extend to the highest and lowest data point. Results were obtained from three independent experiments with at least 8 plants per condition. Asterisks mark statistical significance to NT (MS+ solvents) according to a Wilcoxon-rank test (**0.01; **** 0.0001).

Autophagy regulates rhythmic changes to ARF7 *protein abundance and PBS establishment*

Intrigued by our results showing that co-localization between ARF7 and ATG8a follows rhythmic variation and knowing that *ARF7* expression and protein abundance also shows a similar pattern in the oscillation zone (OZ, Perianez-Rodriguez *et al*, 2021), we decided to explore the impact of autophagy in the natural variation of ARF7's abundance. Therefore, we performed western blots against ARF7 in Col-0 seedlings over time (Fig 4A and Fig EV3) where it can be seen that ARF7 levels displays an oscillatory pattern. Moreover, these results likely explain the variation in co-localization of ARF7-Venus with autophagosomes at different timepoints (Fig 3): condensation is dependent on target concentration (Mcswiggen *et al*, 2019) and therefore more likely observable when ARF7 levels increase. Our findings also illustrate that ARF7 abundance display rhythmic changes that could affect plant tissues outside roots. This is consistent *ARF7*'s expression profile (*e.g.,* Rosado *et al*, 2012; Lee *et al*, 2019) and with ARF7's role during hypocotyl gravi- and phototropism (Wang *et al*, 2020).

In marked contrast, the rhythmic variation in ARF7 abundance was lost ($P \leq 0.05$) when autophagy was disrupted (Fig 4B-E). Moreover, the transcript levels of *LBD16*, which is directly regulated by ARF7, also lost its rhythmic fluctuation in *atg* mutants (Fig 4F). Interestingly, *LBD16* levels are substantially higher in *atg2-1* than Col-0, which could be related to the overall higher levels of ARF7 seen in *atg* mutants. Taken together, these results demonstrate the importance of autophagy in regulating the ARF7-dependent rhythm.

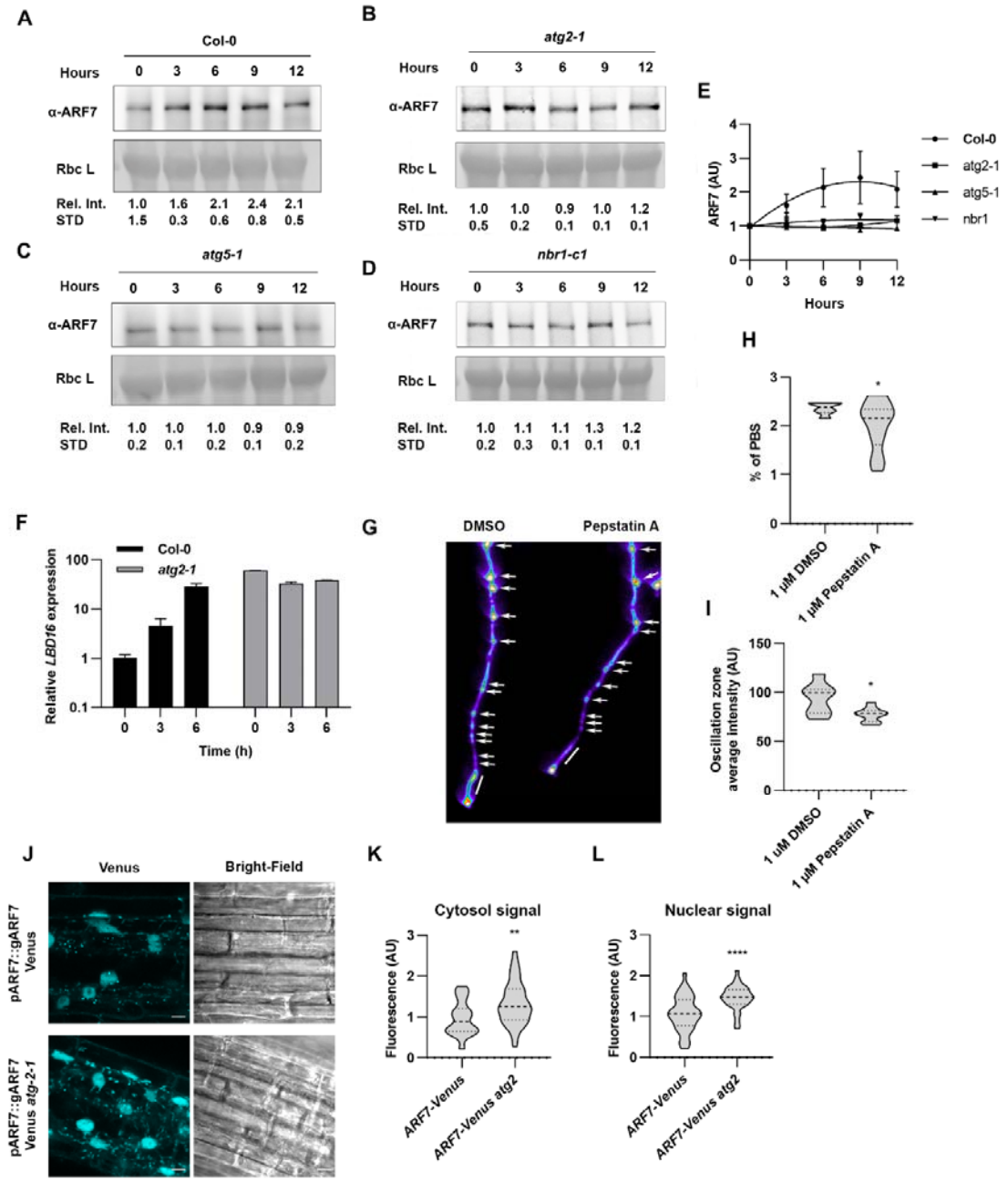

Figure 4: ARF7 abundance displays rhythmic variation and is modulated by autophagy. **A-D)** ARF7 western blots from proteins extracted from Col-0 (**A**); *atg2-1* (**B**); *atg5-1* (**C**) or *nbr1-c1* (**D**) at given hours (hours 0-12). Values below each band represent the relative intensity ratio between ARF7 and RuBisCO large subunit (Rbc L), using Ponceau S as loading control. Ratios were normalized to untreated (NT) which was arbitrarily set to 1. Values given are the mean ± SD of 3 independent experiments, Col-0 was statistically significant (P≤0.05) from all autophagy mutant, according to a Paired-T-test. E) Correlation of the oscillatory pattern for ARF7 protein level over 12h period in in Col 0 and *atg* mutants. **F)** Relative gene expression oscillation of *LBD16* in Col-0 and *atg2-1* at given timepoints. *LBD16* expression was normalized to *ACTIN2* and set to 1 for each genotype at timepoint 0h. **G)** *DR5::Luciferase* images of mock (DMSO) or Pepstatin A (1µM)-grown seedlings depicting PBS (white arrows) and OZ (white bar). **H-I)** Quantification of **H)** PBS (%) and **I)** OZ luminescence intensity depicted from

plants as treated in G. The outline of the violin plots represents the probability of the kernel density. Dotted lines represent interquartile ranges (IQR), with the thick horizontal line representing the median; whiskers extend to the highest and lowest data point. Results represent values from at least 9 plants per condition. Asterisks mark statistical significance to NT according to a Welch t-test (*0.05). **J)** Confocal imaging of ARF7-Venus or *atg2-1* ARF7-Venus in the OZ. **K-L)** Quantification of the fluorescence intensity in cytosol **K**) or nuclei **L**) under the conditions depicted in **H)**. The outline of the violin plots represents the probability of the kernel density. Dotted lines represent interquartile ranges (IQR), with the thick horizontal line representing the median; whiskers extend to the highest and lowest data point. Results were obtained from three independent experiments with at least 8 plants per condition. Asterisks mark statistical significance to NT according to a Mann-Whitney test (**0.005; *** 0.0005).

ARF7 oscillation has been established as an essential step during PBS determination as *arf7-1* mutants display abnormal PBS patterning (Perianez-Rodriguez *et al*, 2021). Because autophagy is necessary for ARF7 turnover (Fig 1-3), we questioned whether PBS establishment could be affected when autophagy is impaired. To track this, we used a reporter line expressing *DR5::Luciferase* and compared PBS numbers and the luminescence intensity in the OZ of seedlings after 7 days treatment with mock (DMSO) or Pepstatin A. As seen in Fig 4G-I, seedlings treated with Pepstatin A had decreased number of PBS and OZ luminescence when compared to the mock-treated samples (P≤0.05). As ARF7 is a repressor of the in-phase oscillations (Perianez-Rodriguez *et al*, 2021), taken together, these results indicate that accumulation of ARF7 due to defective proteostasis leads to decreased *DR5* signal in the OZ and this in turn affects PBS establishment.

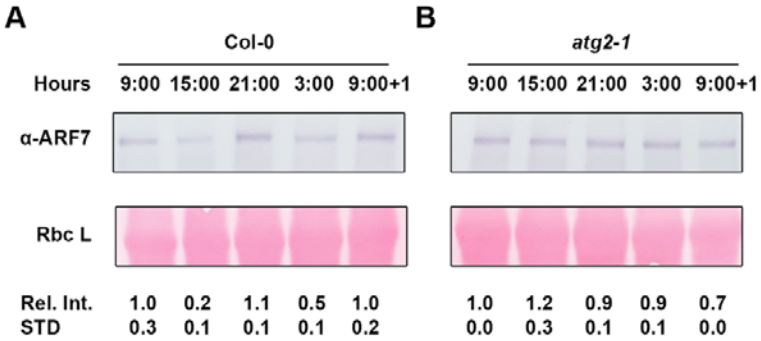

Figure EV 3: ARF7 abundance rhythmically fluctuates over 24 hours and this regulation is lost in *atg2-1*. **A-B)** ARF7 western blots from proteins extracted from Col-0 (**A**) and *atg2-1* (**B**) over a 24h period (09:00 am, 15:00 pm, 21:00pm, 03:00 am and 09:00 am of the following morning). Values below each band represent the relative intensity ratio between ARF7 and RuBisCO large subunit (Rbc L) as stained with Ponceau S used as loading control. Ratios were normalized to untreated (NT) which was arbitrarily set to 1. The experiment was repeated with similar results.

Auxin promoted ARF7 degradation requires functional autophagy

As the root clock oscillations are deeply connected to auxin, we wanted to explore if auxin treatment impacts ARF7 turnover. Consequently, we treated *ARF7-Venus x mCherry ATG8a* seedlings with auxin (Fig 5A-B) for 30 mins as we have previously shown that autophagy is rapidly triggered upon auxin perception (Rodriguez *et al*, 2020). Remarkably, auxin treatment led to rapid and massive ARF7-Venus localization in cytosolic foci, for all tissues tested indicating that auxin promotes ARF7 condensations. Likewise, we also observed a massive increase in mCherry-ATG8 foci (Fig 5), which is consistent with our previous reports showing that quick bursts of auxin lead to rapid increase in autophagic activity (Rodriguez *et al*, 2020). Surprisingly, these dramatic increases of ARF7 and ATG8a cytoplasmic foci only produced a modest, albeit significant, increase in co-localization in the meristem, which contrasts with the strong colocalization observed in the OZ and maturation zone (Fig 5A-B). Given that a) autophagy has a well characterized role in aggregate degradation (*e.g.*, Lim *et al*, 2015); b) the root meristem has been shown to display zone specific chaperonin expression to prevent protein aggregation (Llamas *et al*, 2021); c) ARF7 condensates have liquid and solid properties (Fig EV2, Powers *et al* 2019); d) ARF7 condensates are more prominent in older tissue (Fig 3, Powers *et al*, 2019); our results here likely reveal a mechanism by which auxin treatment leads to a rapid activation of autophagy to modulate ARF7 levels though this mainly occurs in the oscillation and maturation zones, where aggregation is more prone to occur. We also tested whether cytokinin, a hormone often producing contrasting effects to auxin, lead to changes in colocalization between ARF7 and ATG8 (Fig EV4), but this was not the case (P>0.05).

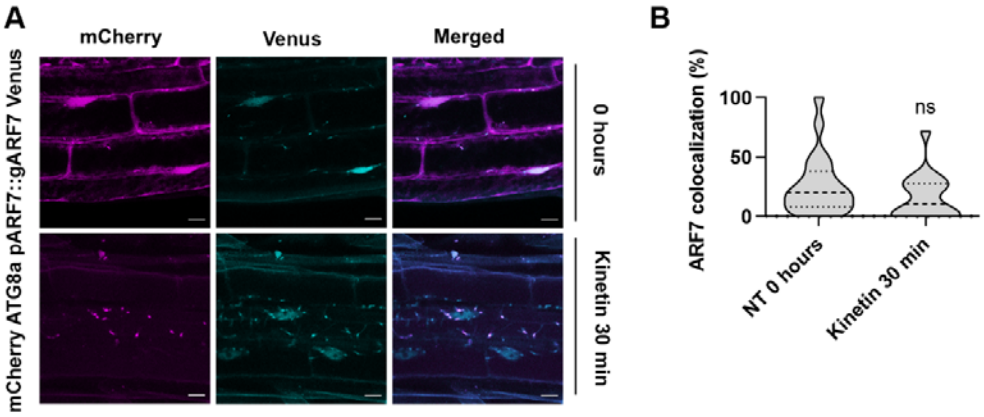

Figure EV 4 Cytokinin has no effect on ARF7 co-localization with autophagosomes. A) Co-localization of ARF7-Venus with mCherry-ATG8a (nuclei and/or cytoplasmic foci) in the maturation zone. MS+ solvent (NT) or 1 µM Kinetin for 30 mins were used for the treatment. Pictures were taken in the respective root zone of 10–14-day old *Arabidopsis* seedlings. Scale bar 10 µM. **B**) Quantification of the co-localization of ARF7-Venus with mCherry-ATG8a. The outline of the violin plots represents the probability of the kernel density. Dotted lines represent interquartile ranges (IQR), with the thick horizontal line representing the median; whiskers extend to the highest and lowest data point. Statistical significance was done according to a Wilcoxon-rank test.

Given that NAA induced rapid ARF7 localization to cytoplasmic foci, we wondered if this would have any effect in ARF7 abundance. Hence, we checked ARF7 levels by western blot with protein extracts from Col-0 and *atg2-1* seedlings treated with NAA for 1h (Fig 5C-D). Our data revealed that NAA produced a mild but significant decrease ($P \leq 0.01$) in ARF7 levels in Col-0, which is consistent with the NAA-induced increase co-localization between ARF7 and autophagic components (Fig 5A-B). In combination, our results (Fig 3-5) support a mechanism by which auxin promotes ARF7 condensation to modulate ARF7 levels, preventing excessive nuclear ARF7 and consequent exaggerated responses. In contrast to previous reports (e.g., Wang *et al*, 2005; Perianez-Rodriguez *et al*, 2021), our data suggests that auxin treatment induces certain changes to ARF7 abundance; which has also been reported at the transcript level after 2h of IAA treatment (Biswas *et al*, 2019). These differences might be easily conciliated due to different experimental set ups among reports: longer auxin treatments (3h-16h), different tissues (*i.e.,* root's OZ or protoplast) and type of auxin were used in those reports (Perianez-Rodriguez *et al*, 2021; Wang *et al*, 2005) as opposed to the experimental setup used here. Concerning *atg2-1* seedlings, NAA treatment did not lead to significant changes in ARF7 levels (Fig 5C-D) which might not be surprising given that ARF7 levels are already elevated when autophagy is impaired and that other compensatory mechanisms (*e.g*., proteasome) could be upregulated to compensate for defective autophagy. Accumulation of ARF7 in the cytoplasm, which we have shown is impacted by autophagy (Fig 1 D-I; Fig 3), has been linked to decreased auxin-dependent responses (Powers *et al*, 2019). As *atg2-1* is unable to execute ARF7 turnover upon rapid auxin treatment (Fig 5), we wondered if this could be indicative of more broad implications, namely altered proteome remodelling during rapid auxin enacted responses. To evaluate this, we gave a short auxin treatment (30 min) to Col-0 and *atg2-1* seedlings and performed Mass Spectrometry (MS). Despite the rapid nature of the treatment with NAA, proteome remodelling was engaged in both genotypes (Fig 5E), and as expected, more proteins were downregulated in Col-0 than *atg2-1* (167 vs 94, Fig 5F). This difference in auxin-induced protein downregulation between genotypes is consistent with the loss of a major proteostasis pathway in the *atg2-1* background. There were also differences, albeit smaller, in what concerns auxin-induced protein accumulation, 146 for Col-0 vs 114 for *atg2-1*. Surprisingly, only around 5% of the proteins with differential regulation upon NAA treatment were similarly down (or up) regulated in both genotypes. These results indicate that while *atg2-1* responds to NAA, the nature of this response is substantially different to that of Col-0, both supporting and expanding our previous findings (Rodriguez *et al* 2020) showing defective NAA-induced reprogramming in *atg* mutants.

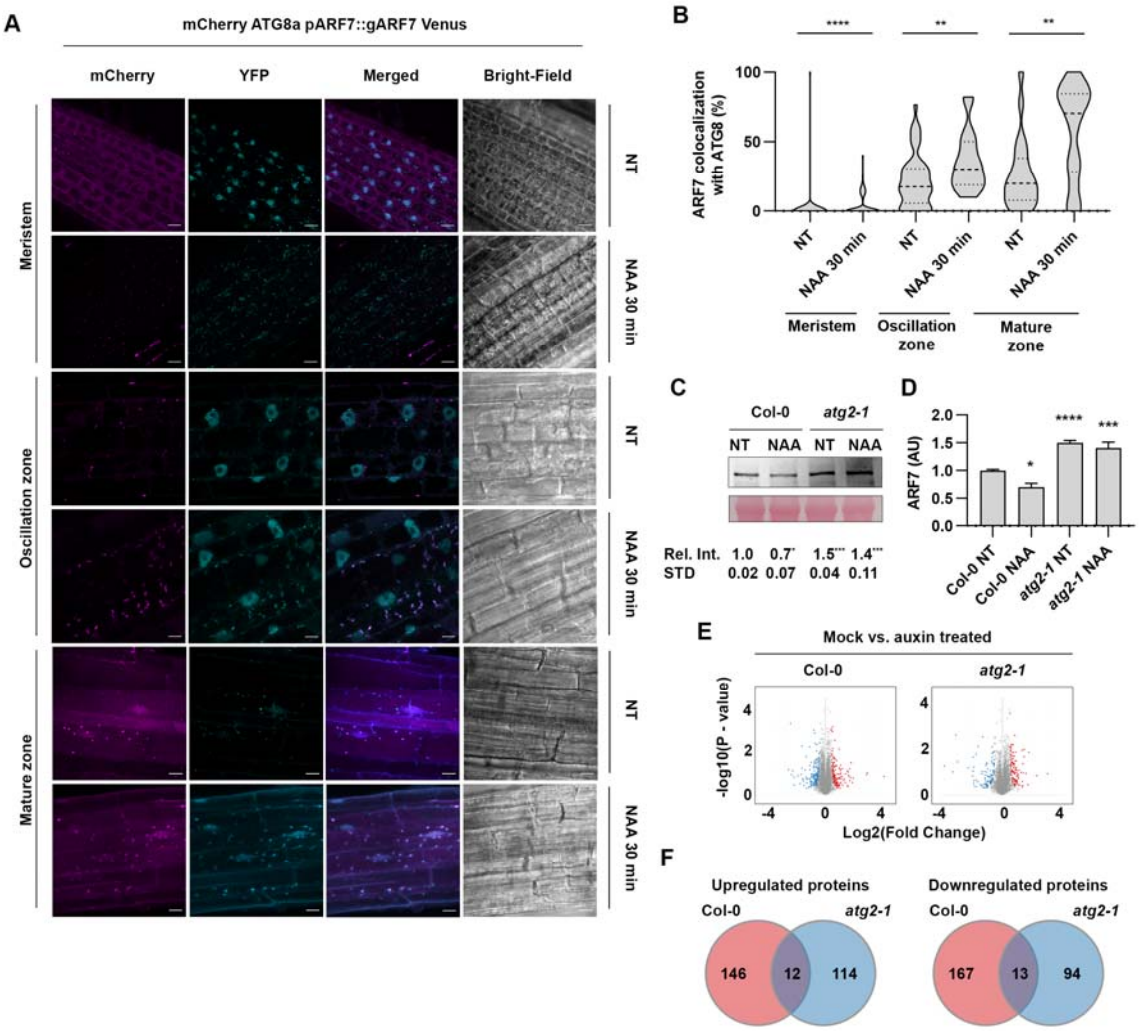

Figure 5 NAA-induces ARF7 condensation and autophagy-mediated degradation. **A**) Co-localization of ARF7-Venus with mCherry-ATG8a (nuclei and/or cytoplasmic foci) in meristem, oscillation or maturation zone after 30min of treatment with 1µM NAA. Pictures were taken in the respective root zone of 10–14-day old *Arabidopsis* seedlings. Scale bar 10 µM. **B**) Quantification of the co-localization of ARF7-Venus with mCherry-ATG8a under conditions depicted in **A)**; The outline of the violin plots represents the probability of the kernel density. Dotted lines represent interquartile ranges (IQR), with the thick horizontal line representing the median; whiskers extend to the highest and lowest data point. Results were obtained from three independent experiments with at least 8 plants per condition. Asterisks mark statistical significance to NT (MS+ solvents) according to a Mann-Whitney U-test (**0.01; **** 0.0001). ARF7 western blot (**C**) and quantification (**D**) from samples extracted from Col-0 or *atg2-1* treated with MS + solvent or MS supplemented with NAA (1µM, 60 min). Values below each band represent the relative intensity ratio between ARF7 and RuBisCO large subunit (Rbc L) as stained with Ponceau S used as loading control. Ratios were normalized to each genotype's NT sample (MS+ solvent), which was set to 1. Values are mean ± SD of 5 biological replicates. Statistical analysis was done using a Holm-Sidak test (* 0.05; *** 0.001). **E)** Volcano plot displaying pairwise protein content changes in Col-0 or *atg2-1*, 30 min after Mock (MS+ EtOH) or NAA treatment (MS+ NAA) with a F.D.R. <0.05 using an unpaired t-test. **F**) Venn diagrams showing the number of differentially expressed proteins overlapping between the datasets (F.D.R. < 0.05).

Autophagy facilitates LR formation

Given that we have seen that autophagy impairment leads to abrogation of ARF7 oscillation and affected PBS establishment, we wondered if accumulation of ARF7 in *atg* mutants could have an impact in other ARF7-dependent phenotypes. Besides PBS, ARF7 regulatory role during LR initiation is also well established (*e.g.,* Okushima *et al*, 2007; Goh *et al*, 2019); consequently, we examined LR production in *atg* mutants by transplanting 5-day old seedlings to vertical plates and scored LRs after 9 days. As shown in Fig 6 (A-B), *atg* mutants have a significantly lower LR density when compared to Col-0. To gain a deeper insight into the impact of defective autophagy-mediated ARF7 homeostasis during LRI we evaluated ARF7-Venus signal in the LRPs of Col-0 and *atg2-1* seedlings. Our analysis revealed that there was significantly more ARF7 signal in *atg2-1* background than in control plants, which is consistent with our data for other root zones (Fig 6 C-D). Importantly, we also observed that while the intensity of ARF7-Venus signal displayed oscillations over time in Col-0 background, this was not the case for *atg2-1* where the intensity of ARF7-Venus signal remaining constant over the same period of time (Fig 6C-D).

Because we have seen that lack of autophagy leads to condensation of ARF7 (Fig 3) which has been linked with decreased auxin responses (Powers *et al*, 2019) and because NAA treatment did not produce major changes to ARF7 abundance in *atg2-1* seedlings (Fig 5C-D), we questioned if *atg* mutants might have impaired auxin responses. To ascertain this, we germinated Col-0 and *atg* mutants and after 5 days, transferred them to vertical MS plates with or without NAA (0.1 µM) and counted LRs 9 days after germination. As seen in Fig 6A-B, NAA treatment caused an increase in LR density for all genotypes, but it did not rescue the differences observed between Col-0 and *atg* mutants. These results agree with our previous findings (Rodriguez *et al*, 2020) regarding *atg* mutants reduced ability to respond effectively to callus inducing media (rich in auxin) to form callus, an *in vitro* process which molecularly resembles lateral root initiation (Sugimoto et al., 2010).

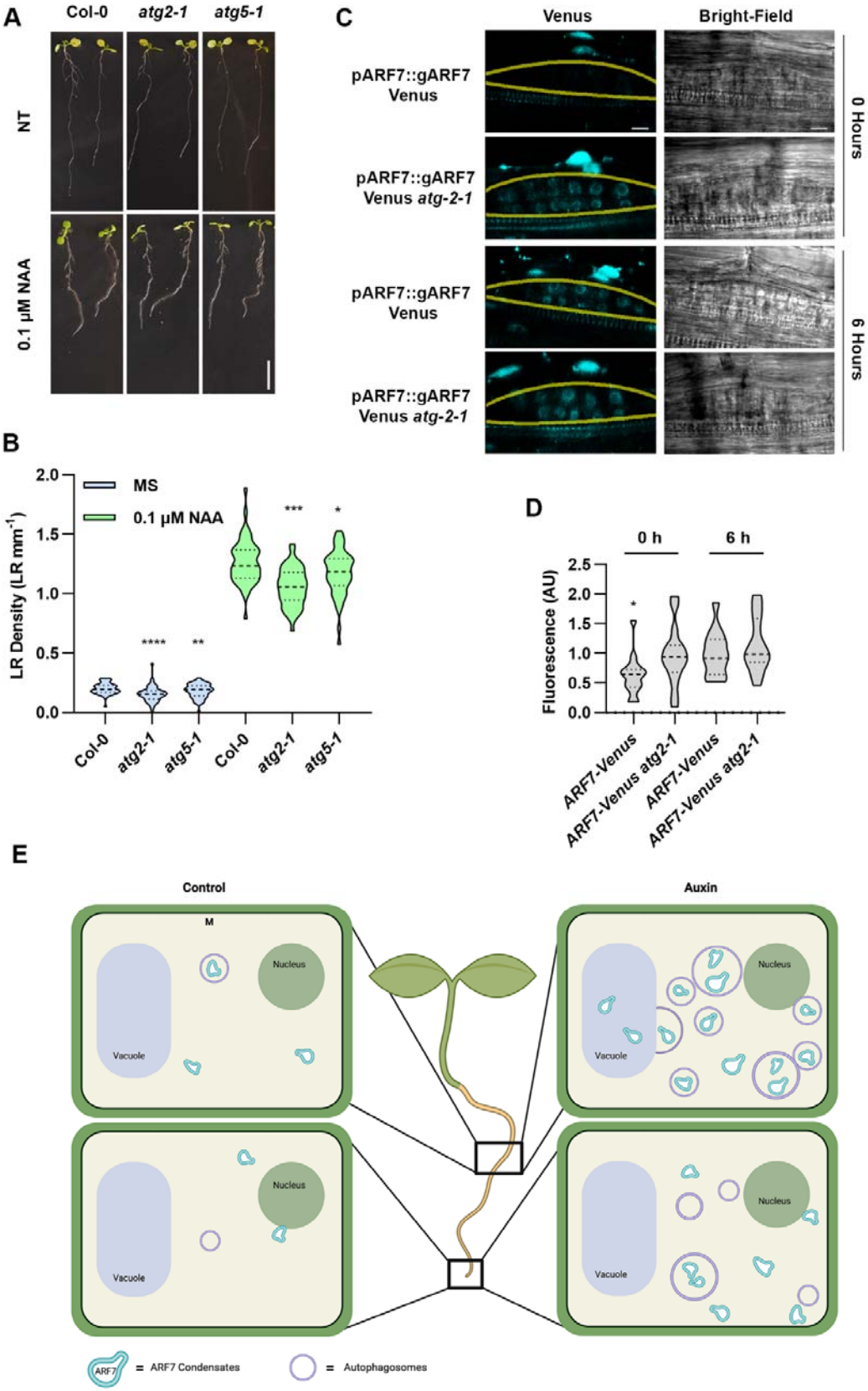
A
Col-0
atg2-1
atg5-1
NT
0.1 µM NAA
C
Venus
Bright-Field
pARF7::gARF7 Venus
pARF7::gARF7 Venus atg-2-1
pARF7::gARF7 Venus
pARF7::gARF7 Venus atg-2-1
0 Hours
6 Hours
B
MS
0.1 µM NAA
LR Density (LR mm-1)
2.0
1.5
1.0
0.5
0.0
****
**
***
*
Col-0
atg2-1
atg5-1
Col-0
atg2-1
atg5-1
D
0 h
6 h
Fluorescence (AU)
2.5
2.0
1.5
1.0
0.5
0.0
*
ARF7-Venus
ARF7-Venus atg2-1
ARF7-Venus
ARF7-Venus atg2-1
E
Control
Auxin
M
Nucleus
Vacuole
Nucleus
Vacuole
Nucleus
Vacuole
Nucleus
Vacuole
ARF7
= ARF7 Condensates
= Autophagosomes

443

Figure 6 Autophagy deficient mutants display impaired proteome remodelling upon auxin treatment and show decreased LR formation capacity **A-B**) LR density quantification in Col-0, *atg2-1* and *atg5-1* grown in MS plates supplemented with Solvent (MS) or 0.1 µM NAA. The outline of the violin plots represents the probability of the kernel density. Dotted lines represent interquartile ranges (IQR), with the thick horizontal line representing the median; whiskers extend to the highest and lowest data point but no more than ±1.5 times the IQR from the box. Results were obtained from three independent experiments with at least 40 plants per condition, asterisks mark statistical significance to Col-0 according to the t-test (*0.05; **** 0.0001). Scale bar: 1 cm). **C-D**) Confocal images of lateral root primordial in Col-0 (top) or *atg2-1* (bottom) expressing *ARF7-Venus* at given time. (**D**) Fluorescence intensity quantification of ARF7-Venus subcellular localization in given lines. The values presented for ARF7-Venus fluorescence intensity in *atg2-1* background were normalized to the values in Col-0 background (which was set to 1). The outline of the violin plots represents the probability of the kernel density. Dotted lines represent interquartile ranges (IQR), with the thick horizontal line representing the median; whiskers extend to the highest and lowest data point. Results were obtained from three independent experiments with at least 7 plants per condition being analysed in total. At least 14 LRPs were measured per genotype/tissue. Asterisks mark statistical significance to NT according to a Welch t-test (*P < 0.05). Yellow line delimits the section (LRP) used for ARF7-Venus quantification **E**) A hypothetical model displaying the tissue and hormone specific regulation of ARF7. The figure was drawn using BioRender (https://www.biorender.com).

Discussion

Here, we show that autophagy modulates ARF7 and ARF19 turnover which would be mediated through the selective cargo adaptor NBR1 (Fig 1 & 2), at least for ARF7. We and others (Jing *et al*, 2022) have shown that MG132 treatment also causes ARF7 to accumulate, which suggests proteasomal activity also regulates this TF turnover. However, care should be taken when inferring proteasomal contribution based solely on MG132-derived data as this inhibitor produces several off-target effects like transcriptional upregulation (Wang *et al*, 2008; Cho *et al*, 2013), interference with lysosomal proteases (Garrison & Bangs, 2020) and autophagosome assembly (Ji *et al*, 2016). Nonetheless, as we see a synergistic effect of MG132 and autophagy inhibition in ARF7 accumulation (Fig 1), it is likely that both degradation pathways are involved in regulating ARFs turnover. The recruitment of both degradation pathways to promote ARF7 turnover is in line with the necessity to keep ARF7 output under tight control (Moreno-Risueño *et al*, 2010; Perianez-Rodriguez *et al*, 2021) and with the fact that excessive activating ARFs lead to dramatic developmental retardation due to exaggerated auxin program execution (Powers *et al*, 2019). Interestingly, we find that while *atg* mutants over accumulate ARF7, autophagy blockage leads to increased ARF7 cytoplasmic condensates and increased ARF7-Venus nuclear signal. Consequently, despite having higher ARF7 levels than Col-0, *atg* mutants show diminished auxin response (Fig 5), PBS establishment (Fig 4), LR formation (Fig 6) and callus formation (Rodriguez *et al*, 2020), a process reminiscent of LR initiation. How does accumulation of ARFs equate to diminished auxin responses? Our data indicates that

autophagy inhibition leads to ARF7 accumulation which may induce supersaturation (Mcswiggen *et al*, 2019) and cause ARF7 condensation in the cytoplasm (Fig 1 & 3). Recent reports (Powers *et al*, 2019; Jing *et al*, 2022) have linked ARFs condensation with decreased auxin responsiveness, therefore, the disruption of protein degradation pathways we report here causes ARF7 levels to increase, promoting cytoplasmic aggregation and consequent reduced auxin responsiveness. ARF7 accumulation and reduced auxin responsiveness might be explained by ARF7's repressor role (Perianez Rodriguez 2021); while ARF7 is needed for auxin responsiveness, ARF7 activity functions in waves and an inability to terminate ARF7 activity maxima likely prevents the plant from executing appropriate auxin induced reprogramming. While our data provides an indication that the mobilization of ARF7 to cytoplasmic foci might be part of a mechanisms aimed at adjusting ARF7 abundance and auxin responsiveness, more experiments are needed to fully understand this process. For instance, Jing *et al*, (2022) recently showed that the loss of function of AFF1 (F-box protein) displays reduced auxin responsiveness due to cytoplasmic hyper condensation and consequent nuclear depletion of ARFs. Despite those dramatic effects, the *aff1* mutants only display mild developmental phenotypes and surprisingly seems able to produce LRs when supplemented with 2-4D; this contrasts with *arf7 x arf19* mutant's severe LR formation defects, even when cultured with auxin (Okushima *et al*, 2007). Moreover, we report that ARF7 cytoplasmic foci do not co-localize with autophagosomes at the same extent in meristem vs more mature tissues, even after inducing ARF7 cytoplasmic condensation with a short NAA treatment (Fig 5). This could be explained by the fact that meristem have an enhanced proteostatic network (Llamas et al 2021) and thus, protein misfolding and aggregation could be less likely to occur. A caveat to this interpretation is that in young tissue, NAA-induced condensates might have greater liquid-like properties, hence the lower co-location with autophagic components. Given that condensate solidification is a progressive process, it is possible with time, ARF7 condensates in young tissue would increase solidity and increase their co-localization with ATG8a/NBR1. In sum, while we provide robust evidence indicating that ARF7 cytoplasmic condensation is part of a triage mechanism for its autophagic degradation, further clarification is needed to completely uncover how this process is regulated in different root zones.

Consistent with defective oscillation of ARF7 levels, *atg* deficiency led to decreased PBS establishment (Fig 4) and LR formation (Fig 6A-B). In the context of LR formation, there is evidence of autophagic participation in a wide range of processes like cell death regulation of endodermal cells above LRPs (Escamez *et al*, 2020) and potentially also during PIN degradation (Kleine-Vehn *et al*, 2008). Moreover, autophagy modulates proteome turnover induced by different hormones like auxin (Fig 5; Rodriguez *et al* 2020), cytokinin

(Acheampong *et al*, 2020; Rodriguez *et al*, 2020) and ABA (Rodriguez *et al*, 2020); all of which are known to influence LR formation. For these reasons, deficiencies in such a transversal process like autophagy complicate result interpretation and ascribing phenotypes to a specific function of autophagy. For instance, ABA is known to interfere with LRs formation (de Smet *et al*, 2003) and consequently, misregulation of ABA signalling in *atg* mutants (Rodriguez *et al*, 2020) could be a source of defective LR formation. However, we have previously seen that *atg* mutants have difficulties forming callus (Rodriguez *et al*, 2020) a process resembling LR initiation and because ABA does not affect callogenesis (Sugimoto *et al*, 2010), it is plausible that LR deficiencies in *atg* mutants occur at an earlier stage than ABA-induced effects (LR emergence). Nonetheless, because our results unequivocally show that autophagy specifically impacts the turnover of the important LR regulators ARF7 and ARF19, it is undeniable that at the very least, defective ARFs turnover in *atg* mutants must contribute to the decreased auxin responses and LR formation we report here (Fig 6E).

In conclusion, we have uncovered a novel role for selective autophagy during post embryonic organ development through the turnover of the key developmental regulators ARF7 and ARF19 and provided further insight into the intricate mechanisms behind ARFs fine-tuning and how this affects root architecture.

Acknowledgements

This work was funded by a Danish Research Agency grant to E.R. (DFF1- 1032-00249B) and Ministerio de Ciencia e Inovacion (MICIN) of Spain and ERDF to M.A.M.-R. (grants PID2019-111523GB-I00 and PID2022-140719NB-I00). We would like to thank Tom Guilfoyle (anti-ARF7 antibody), Koki Yoshimoto (anti-ATG8a antibody), Malcolm Bennett (*pARF7::gARF7-Venus*), Liwen Jiang (*NBR1-C1*) and Hidehiro Fukaki (*pARF19::ARF19-GFP nph4-1 arf19-1*) for sharing material/reagents. We would also like to thank Suksawad Vongvisuttikun for technical assistance, the 2022 classes from the courses “Plant Molecular Biology” & “Experimental Higher Model Organisms” (University of Copenhagen, Denmark) for performing the ARF19-GFP & ARF7-Venus western blots, respectively. Confocal microscopy imaging was performed using equipment from the Center for Advanced Bioimaging (CAB) Denmark, University of Copenhagen. Mass spectrometry analyses were performed by the Proteomics Research Infrastructure (PRI) at the University of Copenhagen (UCPH), supported by the Novo Nordisk Foundation (NNF) (grant agreement number NNF19SA0059305).

Author contributions

Conceptualization: ER; Investigation: ER, EE, JA, AP, HC, JC, PC. Formal analyses: ER, EE, JA, AP, HC, MMR. Writing: ER, EE, JA, NSC, MMR, Visualization: ER, JA; Supervision: ER; MMR Funding acquisition ER. All authors read the manuscript and agreed with the findings reported.

Methods and Materials

Plant material and phenotypic characterization

Arabidopsis seedlings were grown on solid, half-strength MS media (0.8% agar, 1% sucrose at 5.7 pH) and kept at 21 C° with a photoperiod of 16 h (120 µE/m^2/s). Seeds were sterilized with 1.3% bleach followed by 70% alcohol and then rinsed three times with sterilized water. The following lines were used throughout this study; Col-0, *atg2-1* (SALK_076727), *atg5-1* (SAIL_129_B07), *nbr1-c1* (Ji *et al*, 2020), *mCherry ATG8a* & *mCherry NBR1* (Svenning *et al*, 2011), pARF7::gARF7 Venus (Orosa-Puente *et al*, 2018), *pARF19::ARF19-GFP/nph4-1 arf19-1* (Okushima *et al*, 2007); *DR5::Luciferase* (Moreno-Risueno *et al,* 2010).

For the time course experiments, seedlings were acclimated in liquid half-strength MS media for at least 2 days before sampling. The sampling was done just before the chamber light was turned on, and then at indicated times. For LR scoring, seedlings were germinated on half-strength MS media and set to grow vertically for the indicated time. Per genotype, at least 70 plants were analyzed derived from 6 independent experiments. LR's were counted at day 9 as described by (Dubrovsky & Forde, 2012), and only LR's that had at least reached stage IV were included. Per genotype/condition at least 40 plants were counted derived 6 independent experiment. All genotypes were blinded during counting in both assays to prevent potential bias.

Chemical treatments

For confocal microscopy and western blot assays, seedlings were acclimated in liquid half-strength MS media for 2 days acclimation before imaging. For hormone treatment effect on the co-localization of ARF7 with ATG8 & NBR1, samples were either treated with NAA (1 µM), Kinetin (1 µM), or MS for the given time. Chemical inhibition of autophagy was done by pre-treating seedlings with the vacuolar protease inhibitors E-64d (1:3000, stock 10 µM) and Pepstatin A (1 µM) 16 h prior imaging or western blotting. For inhibition of condensates in the mature regions of the root, roots were imaged just before and directly after treatment with condensate inhibitor 1,6-hexanediol (10%) as described by (Wang *et al*, 2021). Images were taken at 5 min interval for 30 min. For PBS determination, seedlings were directly germinated and grown in MS plates supplemented with treatments: Mock, 1 µM Pepstatin A or 10 µM E-64d and grown vertically for 7 days before analyzed.

For protein analysis of ARF7 in *atg* mutants upon proteasomal blockage, samples were treated with or without MG132 (100 µM) for 16 h before harvest.

For luciferase activity imaging, the plates with 7dpi seedlings were sprayed with 1.5 ml of luciferin (D-luciferin potassium salt, Biosynth Carbosynth, Ref: FL08608) 2.5 mM and let to dry. The CCD camera NightOwl and its software IndiGO were used to visualize the reporter *DR5::Luciferase* in the different treatments. We took a luminescence image with 5 minutes of exposition. The images were processed in the software Metamorph Microscopy Automation Software. The same software was used to measure PBS number and Oscillation Zone intensity.

Confocal imaging

Confocal imaging of seedlings was taken with LSM700 Zeiss confocal microscope from the Center for Advanced Bioimaging (CAB) Denmark. Images were taken using 20x air or 63x water objectives. For analysis of ARF7-Venus signal over time, we arbitrarily set the beginning of our experiments to coincide with a time point where ARF7 signal was low. Images were analyzed using Zen Blue 2012 (Zeiss).

Protein extraction

Proteins were extracted using 3xSDS buffer (30% glycerol, 3% SDS, 94 nM Tris, pH 6.8, Bromophenol blue, Complete ultra-tablets EDTA-free protease inhibitor cocktail (Roche), 50mM DTT), then samples were centrifugated for 20 min at 4°C 14000 rpm and the supernatant was moved into a new tube. Samples were denatured at 95°C for 5 min before loaded it for SDS-PAGE.

SDS-PAGE and western blotting

Protein samples were separated in a 4-20% pre-casted gel (Bio-Rad) and transferred overnight onto nitrocellulose membrane (GE Healthcare). Membranes were blocked for 1 h with 5% skim milk (Merck) in TBST [50 mM Tris-HCL, pH 7.5 150 nM NaCl, 0.1% Tween-20 (Sigma)] and incubated 2 h at room temperature or overnight (4°C) with primary antibodies: anti-ARF7 (Wang *et al*, 2005), anti-NBR1 (AS14 2805, Agrisera; 1:5000); anti-GFP (TP401 AMSBio, 1:1000); anti-ATG8a (Yoshimoto *et al*, 2004) Membranes were washed, followed by incubation in anti-rabbit HRP conjugate (Promega; 1:5000). Home-made chemiluminescent substrate (Mruk & Cheng, 2011) was applied before detection. Bands were quantified using ImageJ and normalized to loading controls.

Sample preparation for proteomic analysis

Tissue extracts (100 µg) were diluted in digestion buffer (0.5% SDC in 50 mM TEAB), heat-treated for 5 min at 95 °C, and prepared by a modified filter-aided sample preparation (FASP) protocol (65). In brief, tissue extracts were transferred to 0.5 ml (tilted) spin filters

(Amicon), centrifuged at 14,000g for 15 min, and reduced and alkylated by addition of digestion buffer containing 1:50 (v:v) tris(2-carboxyethyl)phosphine (0.5 M, Sigma) and 1:10 (v:v) 2-chloroacetamide (Sigma) for 30 min at 37 °C. Samples were digested in fresh digestion buffer containing 1 µg Typsin/LysC mix (Promega) and 0.01% ProteaseMAX (Promega) O/N at 37 °C. Digested samples were desalted using stage-tips containing styrene divinylbenzene reversed-phase sulfonate material (SDB-RPS; 3 M).

The mesenteric artery-based library was generated using a pooled digested and stage-tipped sample from the 12-week-old SHRs and WKYs that was fractionated. A high-pH reverse-phase peptide (HpH) fractionation kit (Pierce, Thermo Scientific) was used to create the 15 fractionations.

Data acquisition by liquid chromatography–mass spectrometry (LC-MS)

Peptides were separated on 50 cm columns packed with ReproSil-Pur C18-AQ 1.9 µm resin (Dr Maisch GmbH). Liquid chromatography was performed on an EASY-nLC 1200 ultra-high-pressure system coupled through a nanoelectrospray source to an Exploris 480 mass spectrometer (Thermo Fisher Scientific). Peptides were loaded in buffer A (0.1% formic acid) and separated applying a nonlinear gradient of 5 to 65% buffer B (0.1% formic acid, 80% acetonitrile) at a flow rate of 300 nl/min over 100 min. Spray voltage was set to 2400 V. Data acquisition switched between a full scan (120,000 resolution, 45 ms max. injection time, AGC target 300%) and 49 DIA scans with isolation width of 13.7 m/z and windows overlap of 1 m/z spanning a precursor mass range of 361 to 1033 m/z (15,000 resolution, 22 ms max. injection time, AGC target 1000%). Normalized collision energy was set to 27. All statistical analysis of LFQ derived protein expression data was performed using the automated analysis pipeline of the Clinical Knowledge Graph (Santos *et al*, 2022).

Data availability

The mass spectrometry data from this publication has been deposited to the PRIDE archive (Perez-Riverol *et al* 2022; https://www.ebi.ac.uk/pride/archive/) and given the identifier [PXD042834]

Vector construction and Plant Transformation for BiFC

To create pDEST-ATG8a-SCYNE, pDEST-NBR1-SCYCE, pDEST-ARF7-VYNE and pDEST-TSPO-SCYCE, we PCR amplified (CloneAMP HIFI PCR premix, TAKARA) the coding sequences of *ATG8a*, *NBR1*, *ARF7 and TSPO* flanked recognition sequence for Gateway (Thermofischer) or In-Fusion (Clontech) cloning. *ATG8a, NBR1 and ARF7's* PCR products were cloned into pENTR (Life Technologies) and subsequentially transferred (LR clonase, Invitrogen) into the Gateway-compatible BiFC vectors (Gehl C *et al*, 2009) pDEST-

^{GW} SCYNE, pDEST-^{GW}SCYCE, pDEST-^{GW}VYNE. *TSPO* PCR amplicon was directly cloned into pDEST-^{GW}SCYCE using In-Fusion cloning. *Agrobacterium* strain GV3101 containing constructs were grown in Yeast-extract peptone media supplied with the respective antibiotics overnight. Cultures were spun and resuspended in 10mM $MgCl_2$, 10 mM MES-K and 100 µM acetosyringone to the density of 600nm = 0.15-0.2 per construct and mixed 1:1 and left at room temperature for 2 h, followed by infiltration in 3 weeks old *N. benthamiana*. Pictures were taken 48 hpi using a Zeiss LSM 700 confocal microscope.

Immunoprecipitation

Immunoprecipitation assay was described previously (Zuo *et al*, 2022). In brief, 1 g of 14-day old seedlings were grinded with mortar and pestle and 2 ml of IP extraction buffer (50mM Tris-HCl pH 7.5, 150mM NaCl, 5% glycerol 1mM EDTA, 0.1% NP40, 10mM DTT, protease inhibitor (mini complete ultra, EDTA-free) was added, followed by centrifugation at 4°C 13000 rpm, 20 min. The supernatant was incubated with 20 µl GFP trap beads (Chromotek) rotating for 2-4-hours at 4°C. The beads were washed 3-4 times with washing buffer (20 mM Tris-HCl pH 7.5, 0.15 M NaCl, 0.1% NP40). 30 µL of 3xSDS was added to the beads and heat up 5 min at 95 °C before proceeding for SDS-PAGE.

RNA extraction

RNA was extracted as described previously (Zuo *et al*, 2022) using TRIzol reagent (Thermo Scientific), treated with DNase (Thermo Scientific) and was reverse transcribed into cDNA using Reverse Aid kit (Thermo Scientific) as described by the manufacturer. qPCR assays were executed on the Quantstudio 1 (Applied Biosystems) system using SYBR Green master mix (ThermoFisher), *ACT2* was used as internal control. All primers used for qPCR analysis are listed in Supplementary table 1. The experiment was repeated three times.

Supplementary table 1

Cloning primers	
ARF7 Forward primer	5'-CACCATGAAAGCTCCTTCATCAA-3'
ARF7 Reverse primer	5'-TCACCGGTTAAACGAAGTGGC-3'
NBR1 Forward primer	5'-CACCATGGAGTCTACTGCTA-3'
NBR1 Reverse primer	5'-TCAAGCCTCCTTCTCCCCT-3'
TSPO Forward primer	5'-GCAGGCTCCGCGGCCATGGATTCTCAGGACATCAGA-3'
TSPO Reverse primer	5'-AGCTGGGTCGGCGCGTCACGCGACTGCAAGCTTTAC-3'
ATG8a Forward	5'-CACCATGATCTTTGCTTGCTTGA-3'

ATG8a Reverse	5’-TCATCAAGCAACGGTAAGAGAT-3’
qPCR primers	
ACT2 Forward primer	5’-CTTGTTCCAGCCCTCGTTTGTG-3’
ACT2 Reverse primer	5’-CCTTGGAGATCCACATCTGCTG-3’
ARF7 Forward primer	5’-CAAGGTCACAGTGAGCAAGTCG -3’
ARF7 Reverse primer	5’-TGTGGAGCATGCATATGAGCTTGG -3’
LBD16 Forward primer	5’-TCCATGATCGATGTGAAGCTGTCG-3’
LBD16 Reverse primer	5’-TGTGATTGCAAGAAAGCCACCTG-3’

References

Bassham DC, Laporte M, Marty F, Moriyasu Y, Ohsumi Y, Olsen LJ & Yoshimoto K (2006) Autophagy in development and stress responses of plants. *Autophagy* 2: 2–11

Biswas MS, Fukaki H, Mori IC, Nakahara K & Ichi Mano J' (2019) Reactive oxygen species and reactive carbonyl species constitute a feed-forward loop in auxin signaling for lateral root formation. *The Plant Journal* 100: 536–548

Chen L, Liao B, Qi H, Xie LJ, Huang L, Tan WJ, Zhai N, Yuan LB, Zhou Y, Yu LJ, *et al* (2015) Autophagy contributes to regulation of the hypoxia response during submergence in Arabidopsis thaliana. *Autophagy* 11: 2233–2246

Cho KS, Kwon KJ, Jeon SJ, Joo SH, Kim KC, Cheong JH, Bahn GH, Kim HY, Han SH, Shin CY, *et al* (2013) Transcriptional Upregulation of Plasminogen Activator Inhibitor-1 in Rat Primary Astrocytes by a Proteasomal Inhibitor MG132. *Biomol Ther (Seoul)* 21: 107

Coll NS, Smidler A, Puigvert M, Popa C, Valls M, Dangl JL (2014). The plant metacaspase AtMC1 in pathogen-triggered programmed cell death and aging: functional linkage with autophagy. Cell Death Differ. 2014 Sep;21(9):1399-408.

Deb S, Sankaranarayanan S, Wewala G, Widdup E & Samuel MA (2014) The S-Domain Receptor Kinase Arabidopsis Receptor Kinase2 and the U Box/Armadillo Repeat-Containing E3 Ubiquitin Ligase9 Module Mediates Lateral Root Development under Phosphate Starvation in Arabidopsis. *Plant Physiol* 165: 1647–1656

Du Y & Scheres B (2018) Lateral root formation and the multiple roles of auxin. *J Exp Bot* 69: 155–167

Dubrovsky JG & Forde BG (2012) Quantitative analysis of lateral root development: Pitfalls and how to avoid them. *Plant Cell* 24: 4–14

Escamez S, André D, Sztojka B, Bollhöner B, Hall H, Berthet B, Voß U, Lers A, Maizel A, Andersson M, *et al* (2020) Cell Death in Cells Overlying Lateral Root Primordia Facilitates Organ Growth in Arabidopsis. *Current Biology* 30: 455-464.e7

Fujioka Y, Alam JM, Noshiro D, Mouri K, Ando T, Okada Y, May AI, Knorr RL, Suzuki K, Ohsumi Y, *et al* (2020) Phase separation organizes the site of autophagosome formation. *Nature* 578: 301–305

Garrison P & Bangs JD (2020) p97 Inhibitor CB-5083 Blocks ERAD in Trypanosoma brucei. *Mol Biochem Parasitol* 239

Gehl C, Waadt R, Kudla J, Mendel R & Hansch R (2009) New GATEWAY vectors for high throughput analyses of protein-protein interactions by bimolecular fluorescence complementation. *Mol Plant*: 1051–1058

Goh T, Toyokura K, Yamaguchi N, Okamoto Y, Uehara T, Kaneko S, Takebayashi Y, Kasahara H, Ikeyama Y, Okushima Y, *et al* (2019) Lateral root initiation requires the sequential induction of transcription factors LBD16 and PUCHI in Arabidopsis thaliana. *New Phytologist* 224: 749–760

Hachez C, Veljanovski V, Reinhardt H, Guillaumot D, Vanhee C, Chaumont F & Batoko H (2014) The Arabidopsis abiotic stress-induced TSPO-Related protein reduces cell-surface expression of the aquaporin PIP2;7 through protein-protein interactions and autophagic degradation. *Plant Cell* 26: 4974–4990

Hafrén A, Macia J-L, Love AJ, Milner JJ, Drucker M & Hofius D (2017) Selective autophagy limits cauliflower mosaic virus infection by NBR1-mediated targeting of viral capsid protein and particles. *Proceedings of the National Academy of Sciences* 114: E2026–E2035

Hofius D, Schultz-Larsen T, Joensen J, Tsitsigiannis DI, Petersen NHTT, Mattsson O, Jørgensen LB, Jones JDGG, Mundy J & Petersen M (2009) Autophagic Components Contribute to Hypersensitive Cell Death in Arabidopsis. *Cell* 137: 773–783

Huang L, Yu LJ, Zhang X, Fan B, Wang FZ, Dai YS, Qi H, Zhou Y, Xie LJ & Xiao S (2019) Autophagy regulates glucose-mediated root meristem activity by modulating ROS production in Arabidopsis. *Autophagy* 15: 407–422

Jacomin AC, Samavedam S, Promponas V & Nezis IP (2016) iLIR database: A web resource for LIR motif-containing proteins in eukaryotes. *Autophagy* 12: 1945–1953

Ji C, Zhou J, Guo R, Lin Y, Kung C-H, Hu S, Ng WY, Zhuang X & Jiang L (2020) AtNBR1 Is a Selective Autophagic Receptor for AtExo70E2 in Arabidopsis. *Plant Physiol* 184: 777–791

Ji MM, Lee JM, Mon H, Xu J, Tatsuke T & Kusakabe T (2016) Proteasome inhibitor MG132 impairs autophagic flux through compromising formation of autophagosomes in Bombyx cells. *Biochem Biophys Res Commun* 479: 690–696

Jing H, Korasick DA, Emenecker RJ, Morffy N, Wilkinson EG, Powers SK & Strader LC (2022) Regulation of AUXIN RESPONSE FACTOR condensation and nucleo-cytoplasmic partitioning. *Nat Commun* 13: 4015

Kanne J V., Ishikawa M, Bressendorff S, Ansbøl J, Hasebe M, Rodriguez E & Petersen M (2021) Overexpression of ATG8/LC3 enhances wound-induced somatic reprogramming in Physcomitrium patens. *Autophagy* 18: 1463–1466

Kirkin V, Lamark T, Sou YS, Bjørkøy G, Nunn JL, Bruun JA, Shvets E, McEwan DG, Clausen TH, Wild P, *et al* (2009) A Role for NBR1 in Autophagosomal Degradation of Ubiquitinated Substrates. *Mol Cell* 33: 505–516

Kleine-Vehn J, Leitner J, Zwiewka M, Sauer M, Abas L, Luschnig C & Friml J (2008) Differential degradation of PIN2 auxin efflux carrier by retromer-dependent vacuolar targeting. *Proceedings of the National Academy of Sciences of the USA* 105: 17812–17817

Lee HW, Cho C, Pandey SK, Park Y, Kim M-J & Kim J (2019) LBD16 and LBD18 acting downstream of ARF7 and ARF19 are involved in adventitious root formation in Arabidopsis. *BMC Plant Biology* 19: 1–11

Levine B & Klionsky DJ (2004) Development by Self-Digestion. *Dev Cell* 6: 463–477

Lim J, Lachenmayer ML, Wu S, Liu W & Kundu M (2015) Proteotoxic Stress Induces Phosphorylation of p62 / SQSTM1 by ULK1 to Regulate Selective Autophagic Clearance of Protein Aggregates. 1–28

Liu EY, Xu N, O'Prey J, Lao LY, Joshi S, Long JS, O'Prey M, Croft DR, Beaumatin F, Baudot AD, *et al* (2015) Loss of autophagy causes a synthetic lethal deficiency in DNA repair. *Proceedings of the National Academy of Sciences* 112: 773–778

Liu Y, Xiong Y & Bassham DC (2009) Autophagy is required for tolerance of drought and salt stress in plants. *Autophagy* 5: 954–963

Llamas E, Torres-Montilla S, Lee HJ, Barja MV, Schlimgen E, Dunken N, Wagle P, Werr W, Zuccaro A, Rodríguez-Concepción M, *et al* (2021) The intrinsic chaperone network of Arabidopsis stem cells confers protection against proteotoxic stress. *Aging Cell* 20: 1–12

Lv B, Wei K, Hu K, Tian T, Zhang F, Yu Z, Zhang D, Su Y, Sang Y, Zhang X, *et al* (2021) MPK14-mediated auxin signaling controls lateral root development via ERF13-regulated very-long-chain fatty acid biosynthesis. *Mol Plant* 14: 285–297

Mcswiggen DT, Mir M, Darzacq X & Tjian R (2019) Evaluating phase separation in live cells: diagnosis, caveats, and functional consequences. *Genes Dev* 33: 1619–1634

Moreno-Risueño MA, Van Norman JM, Moreno A, Zhang J, Ahnert SE & Benfey PN (2010) Oscillating Gene Expression Determines Competence for Periodic Arabidopsis Root Branching. *Science (1979)* 329: 1306–1311

Mruk DD & Cheng CY (2011) Enhanced chemiluminescence (ECL) for routine immunoblotting. *Spermatogenesis* 1: 121–122

Munch D, Rodriguez E, Bressendorff S, Park OK, Hofius D & Petersen M (2014) Autophagy deficiency leads to accumulation of ubiquitinated proteins, ER stress, and cell death in Arabidopsis. *Autophagy* 10: 1579–1587

Nolan TM, Brennan B, Yang M, Chen J, Zhang M, Li Z, Wang X, Bassham DC, Walley J & Yin Y (2017) Selective Autophagy of BES1 Mediated by DSK2 Balances Plant Growth and Survival. *Dev Cell* 41: 33-46.e7

Okushima Y, Fukaki H, Onoda M, Theologis A & Tasaka M (2007) ARF7 and ARF19 regulate lateral root formation via direct activation of LBD/ASL genes in Arabidopsis. *Plant Cell* 19: 118–130

Orosa-Puente B, Leftley N, von Wangenheim D, Banda J, Srivastava AK, Hill K, Truskina J, Bhosale R, Morris E, Srivastava M, *et al* (2018) Root branching toward water involves posttranslational modification of transcription factor ARF7. *Science* 362: 1407–1410

Perez-Garcia P, Serrano-Ron L, Moreno-Risueno MA (2022) The nature of the root clock at single cell resolution: Principles of communication and similarities with plant and animal pulsatile and circadian mechanisms. Curr Opin Cell Biol. Aug;77:102102.

Perez-Riverol Y, Bai J, Bandla C, Hewapathirana S, García-Seisdedos D, Kamatchinathan S, Kundu D, Prakash A, Frericks-Zipper A, Eisenacher M, Walzer M, Wang S, Brazma A, Vizcaíno JA (2022). The PRIDE database resources in

2022: A Hub for mass spectrometry-based proteomics evidences. Nucleic Acids Res 50(D1):D543-D552.

Perianez-Rodriguez J, Rodriguez M, Marconi M, Bustillo-Avendaño E, Wachsman G, Sanchez-Corrionero A, De Gernier H, Cabrera J, Perez-Garcia P, Gude I, *et al* (2021) An auxin-regulable oscillatory circuit drives the root clock in Arabidopsis. *Sci Adv* 7

Powers SK, Holehouse AS, Korasick DA, Schreiber KH, Clark NM, Jing H, Emenecker R, Han S, Tycksen E, Hwang I, *et al* (2019) Nucleo-cytoplasmic Partitioning of ARF Proteins Controls Auxin Responses in Arabidopsis thaliana. *Mol Cell* 76: 177–190

Rodriguez E, Chevalier J, Olsen J, Ansbøl J, Kapousidou V, Zuo Z, Svenning S, Loefke C, Koemeda S, Drozdowskyj PS, *et al* (2020) Autophagy mediates temporary reprogramming and dedifferentiation in plant somatic cells. *EMBO J* 39: e103315

Rosado A, Li R, van de Ven W, Hsu E & Raikhel N V. (2012) Arabidopsis ribosomal proteins control developmental programs through translational regulation of auxin response factors. *Proceedings of the National Academy of Sciences* 109: 19537–19544

Santos A, Colaço AR, Nielsen AB, Niu L, Strauss M, Geyer PE, Coscia F, Albrechtsen NJW, Mundt F, Jensen LJ, *et al* (2022) A knowledge graph to interpret clinical proteomics data. *Nat Biotechnol* 40: 692–702

Scott RC, Schuldiner O & Neufeld TP (2004) Role and Regulation of Starvation-Induced Autophagy in the Drosophila Fat Body. *Dev Cell* 7: 167–178

Sedaghatmehr M, Thirumalaikumar VP, Kamranfar I, Marmagne A, Masclaux-Daubresse C & Balazadeh S (2019) A regulatory role of autophagy for resetting the memory of heat stress in plants. *Plant Cell Environ* 42: 1054–1064

Stephani M, Picchianti L, Gajic A, Beveridge R, Skarwan E, Hernandez VS de M, Mohseni A, Clavel M, Zeng Y, Naumann C, *et al* (2020) A cross-kingdom conserved ER-phagy receptor maintains endoplasmic reticulum homeostasis during stress. *Elife* 9: 1–105

Sugimoto K, Jiao Y & Meyerowitz EM (2010) Arabidopsis Regeneration from Multiple Tissues Occurs via a Root Development Pathway. *Dev Cell* 18: 463–471

Svenning S, Lamark T, Krause K & Johansen T (2011) Plant NBR1 is a selective autophagy substrate and a functional hybrid of the mammalian autophagic adapters NBR1 and p62/SQSTM1. *Autophagy* 7: 993–1010

Tarnowski L, Rodriguez MC, Brzywczy J, Piecho-Kabacik M, Krčkova Z, Martinec J, Wawrzynska A & Sirko A (2020) A selective autophagy cargo receptor NBR1 modulates abscisic acid signalling in Arabidopsis thaliana. *Sci Rep* 10: 7778

Turco E, Savova A, Gere F, Ferrari L, Romanov J, Schuschnig M, Martens S & Savova A (2021) Reconstitution defines the roles of p62, NBR1 and TAX1BP1 in ubiquitin condensate formation and autophagy initiation. *Nat Commun* 12: 5212

Ulmasov T, Hagen G & Guilfoyle TJ (1997) ARF1, a transcription factor that binds to auxin response elements. *Science (1979)* 276: 1865–1868

Vanhee C, Zapotoczny G, Masquelier D, Ghislain M & Batoko H (2011) The Arabidopsis Multistress Regulator TSPO Is a Heme Binding Membrane Protein and a Potential Scavenger of Porphyrins via an Autophagy-Dependent Degradation Mechanism. *Plant Cell* 23: 785–805

Wachsman G, Zhang J, Moreno-Risueño MA, Anderson CT & Benfey PN (2020) Cell wall remodeling and vesicle trafficking mediate the root clock in *Arabidopsis*. *Science* 370: 819–823

Wang HQ, Liu HM, Zhang HY, Guan Y & Du ZX (2008) Transcriptional upregulation of BAG3 upon proteasome inhibition. *Biochem Biophys Res Commun* 365: 381–385

Wang S, Tiwari SB, Hagen G & Guilfoyle TJ (2005) AUXIN RESPONSE FACTOR7 Restores the Expression of Auxin-Responsive Genes in Mutant Arabidopsis Leaf Mesophyll Protoplasts. *Plant Cell* 17: 1979–1993

Wang X, Jiang B, Gu L, Gu L, Chen Y, Mora M, Zhu M, Noory E, Wang Q & Lin C (2021) A photoregulatory mechanism of the circadian clock in Arabidopsis. *Nat Plants* 7: 1397–1408

Wang X, Yu R, Wang J, Lin Z, Han X, Deng Z, Fan L, He H, Deng XW & Chen H (2020) The Asymmetric Expression of SAUR Genes Mediated by ARF7/19 Promotes the Gravitropism and Phototropism of Plant Hypocotyls. *Cell Rep* 31: 107529

Wu J, Michaeli S, Picchianti L, Dagdas Y, Galili G & Peled-Zehavi H (2021) ATI1 (ATG8-interacting protein 1) and ATI2 define a plant starvation-induced reticulophagy pathway and serve as MSBP1/MAPR5 cargo receptors. *Autophagy* 17: 3375–3388

Xie D, Chen M, Niu J, Wang L, Li Y, Fang X, Li P & Qi Y (2021) Phase separation of SERRATE drives dicing body assembly and promotes miRNA processing in Arabidopsis. *Nat Cell Biol* 23: 32–39

Yoshii SR, Kuma A, Akashi T, Hara T, Yamamoto A, Kurikawa Y, Itakura E, Tsukamoto S, Shitara H, Eishi Y, *et al* (2016) Systemic Analysis of Atg5-Null Mice Rescued from Neonatal Lethality by Transgenic ATG5 Expression in Neurons. *Dev Cell* 39: 116–130

Zhang Y, Yan L, Zhou Z, Yang P, Tian E, Zhang K, Zhao Y, Li Z, Song B, Han J, *et al* (2009) SEPA-1 Mediates the Specific Recognition and Degradation of P Granule Components by Autophagy in C. elegans. *Cell* 136: 308–321

Zhou J, Wang J, Cheng Y, Chi YJ, Fan B, Yu JQ & Chen Z (2013a) NBR1-Mediated Selective Autophagy Targets Insoluble Ubiquitinated Protein Aggregates in Plant Stress Responses. *PLoS Genet* 9: 1004477

Zhou J, Wang J, Cheng Y, Chi YJ, Fan B, Yu JQ & Chen Z (2013b) NBR1-Mediated Selective Autophagy Targets Insoluble Ubiquitinated Protein Aggregates in Plant Stress Responses. *PLoS Genet* 9: 1004477

Zhou J, Zhang Y, Qi J, Chi Y, Fan B, Yu JQ & Chen Z (2014) E3 Ubiquitin Ligase CHIP and NBR1-Mediated Selective Autophagy Protect Additively against Proteotoxicity in Plant Stress Responses. *PLoS Genet* 10: e1004116

Zuo Z, Roux M, Rodriguez E & Petersen M (2022) mRNA Decapping Factors LSM1 and PAT Paralogs Are Involved in Turnip Mosaic Virus Viral Infection. *Molecular Plant-Microbe Interactions* 5: 125–129

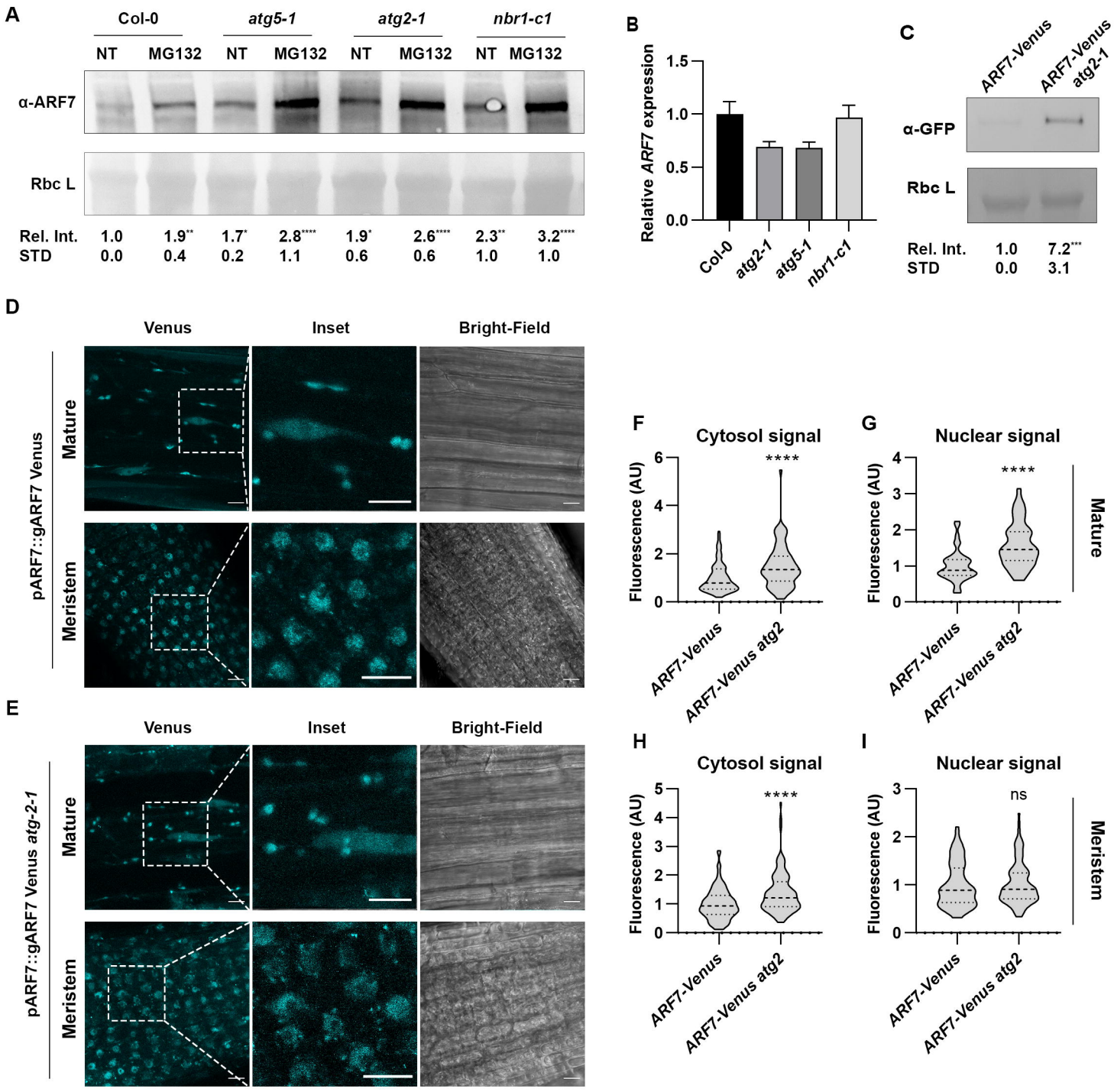
A
Col-0
atg5-1
atg2-1
nbr1-c1
NT
MG132
α-ARF7
Rbc L
Rel. Int. 1.0 1.9** 1.7* 2.8**** 1.9* 2.6**** 2.3** 3.2****
STD 0.0 0.4 0.2 1.1 0.6 0.6 1.0 1.0
B
Relative ARF7 expression
1.5
1.0
0.5
0.0
Col-0
atg2-1
atg5-1
nbr1-c1
C
ARF7-Venus
ARF7-Venus atg2-1
α-GFP
Rbc L
Rel. Int. 1.0 7.2***
STD 0.0 3.1
D
Venus
Inset
Bright-Field
pARF7::gARF7 Venus
Mature
Meristem
E
pARF7::gARF7 Venus atg-2-1
F
Cytosol signal
Fluorescence (AU)
****
ARF7-Venus
ARF7-Venus atg2
G
Nuclear signal
Mature
H
I
ns
Meristem

Figure 2

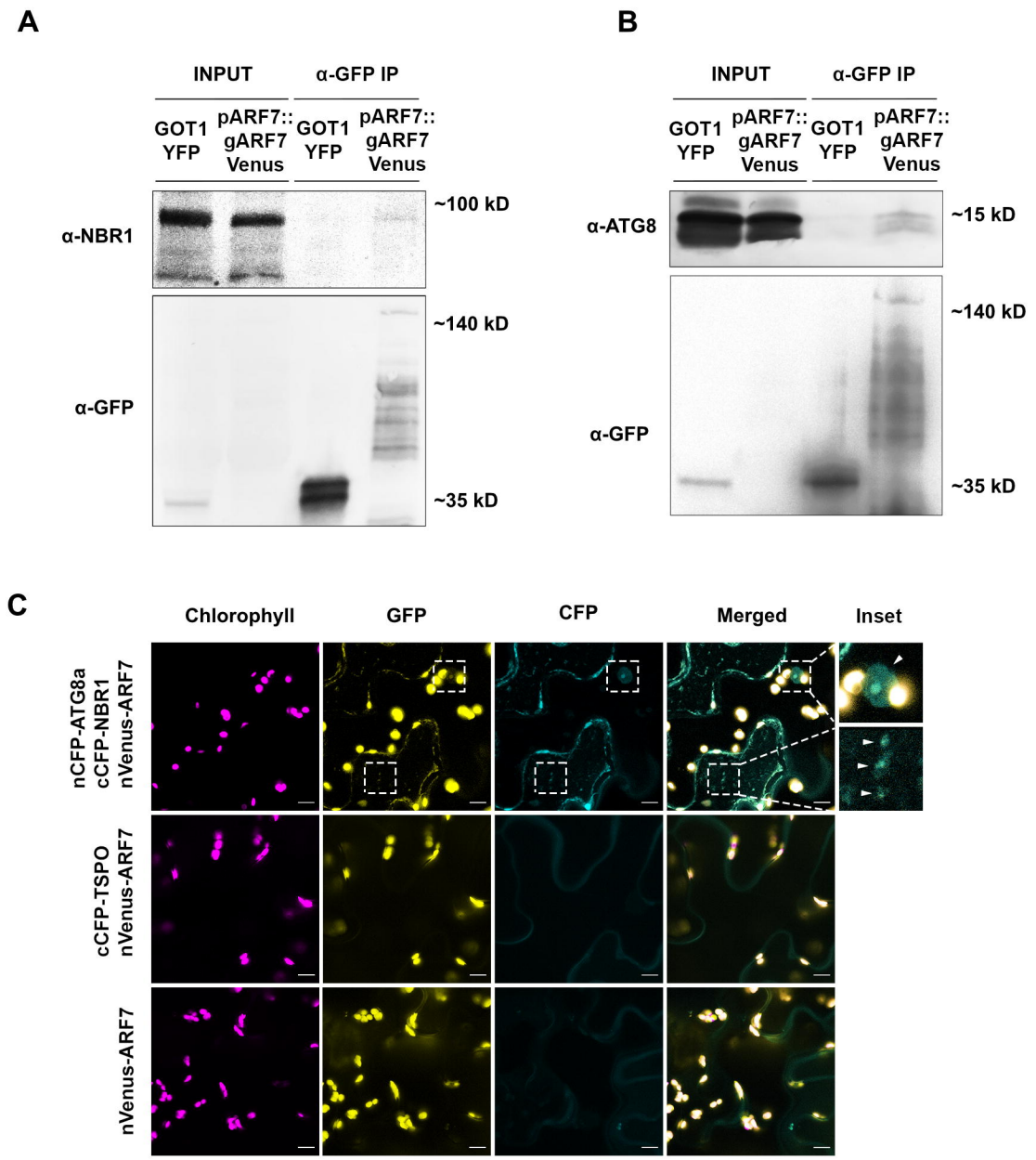
A
INPUT
α-GFP IP
GOT1 YFP
pARF7:: gARF7 Venus
GOT1 YFP
pARF7:: gARF7 Venus
α-NBR1
~100 kD
α-GFP
~140 kD
~35 kD
B
INPUT
α-GFP IP
GOT1 YFP
pARF7:: gARF7 Venus
GOT1 YFP
pARF7:: gARF7 Venus
α-ATG8
~15 kD
α-GFP
~140 kD
~35 kD
C
Chlorophyll
GFP
CFP
Merged
Inset
nCFP-ATG8a
cCFP-NBR1
nVenus-ARF7
cCFP-TSPO
nVenus-ARF7
nVenus-ARF7

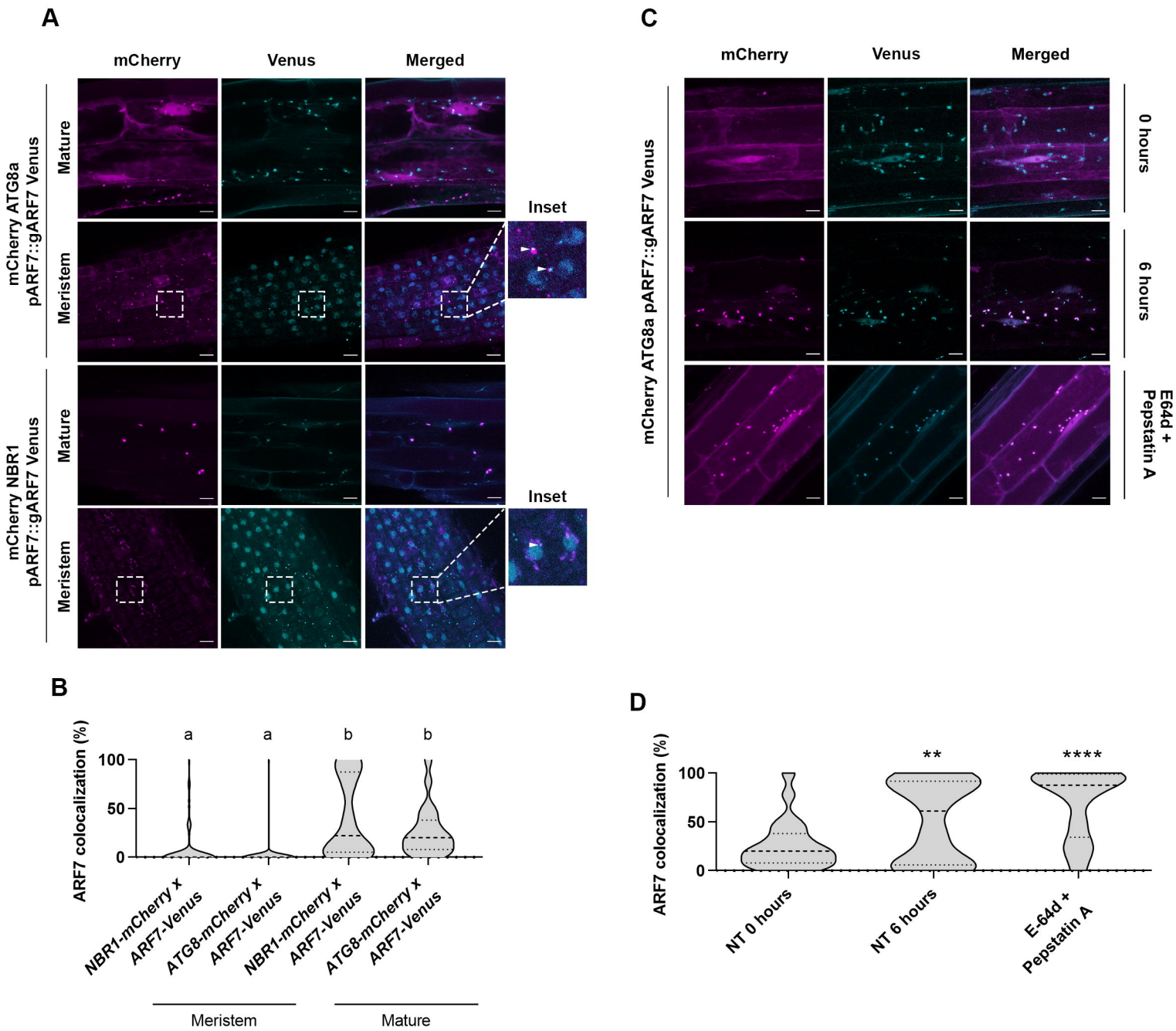
A
mCherry
Venus
Merged
mCherry ATG8a pARF7::gARF7 Venus
Mature
Meristem
Inset
mCherry NBR1 pARF7::gARF7 Venus
Mature
Meristem
Inset
C
mCherry
Venus
Merged
mCherry ATG8a pARF7::gARF7 Venus
0 hours
6 hours
E64d + Pepstatin A
B
ARF7 colocalization (%)
100
50
0
a
a
b
b
NBR1-mCherry x ARF7-Venus
ATG8-mCherry x ARF7-Venus
NBR1-mCherry x ARF7-Venus
ATG8-mCherry x ARF7-Venus
Meristem
Mature
D
ARF7 colocalization (%)
100
50
0
**
****
NT 0 hours
NT 6 hours
E-64d + Pepstatin A

Figure 4

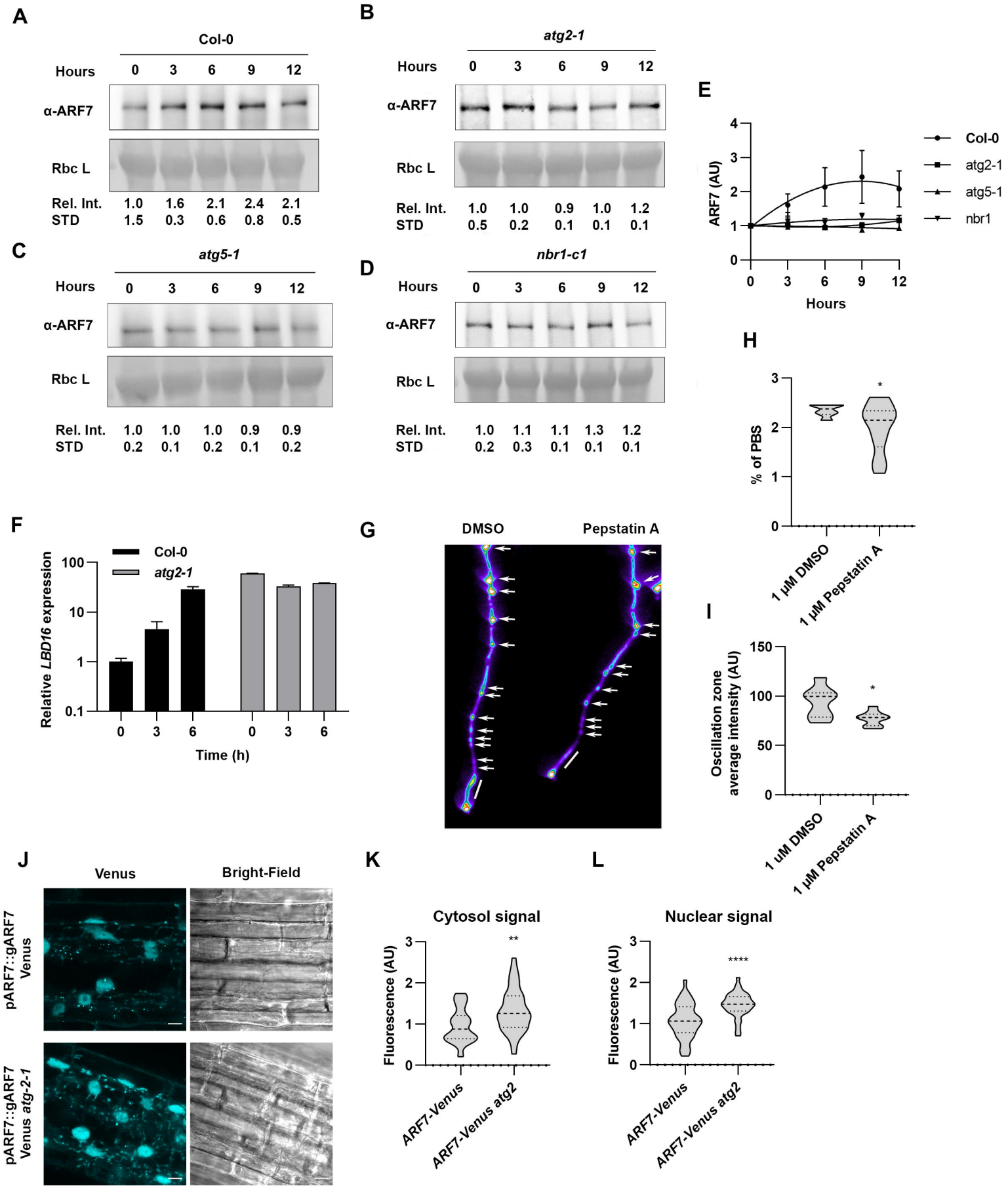
A
Col-0
Hours 0 3 6 9 12
α-ARF7
Rbc L
Rel. Int. 1.0 1.6 2.1 2.4 2.1
STD 1.5 0.3 0.6 0.8 0.5
B
atg2-1
Hours 0 3 6 9 12
α-ARF7
Rbc L
Rel. Int. 1.0 1.0 0.9 1.0 1.2
STD 0.5 0.2 0.1 0.1 0.1
C
atg5-1
Hours 0 3 6 9 12
α-ARF7
Rbc L
Rel. Int. 1.0 1.0 1.0 0.9 0.9
STD 0.2 0.1 0.2 0.1 0.2
D
nbr1-c1
Hours 0 3 6 9 12
α-ARF7
Rbc L
Rel. Int. 1.0 1.1 1.1 1.3 1.2
STD 0.2 0.3 0.1 0.1 0.1
E
ARF7 (AU)
Hours
Col-0
atg2-1
atg5-1
nbr1
F
Relative LBD16 expression
Col-0
atg2-1
Time (h)
G
DMSO
Pepstatin A
H
% of PBS
1 µM DMSO
1 µM Pepstatin A
I
Oscillation zone average intensity (AU)
1 uM DMSO
1 µM Pepstatin A
J
Venus
Bright-Field
pARF7::gARF7 Venus
pARF7::gARF7 Venus atg-2-1
K
Cytosol signal
Fluorescence (AU)
ARF7-Venus
ARF7-Venus atg2
L
Nuclear signal
Fluorescence (AU)
ARF7-Venus
ARF7-Venus atg2

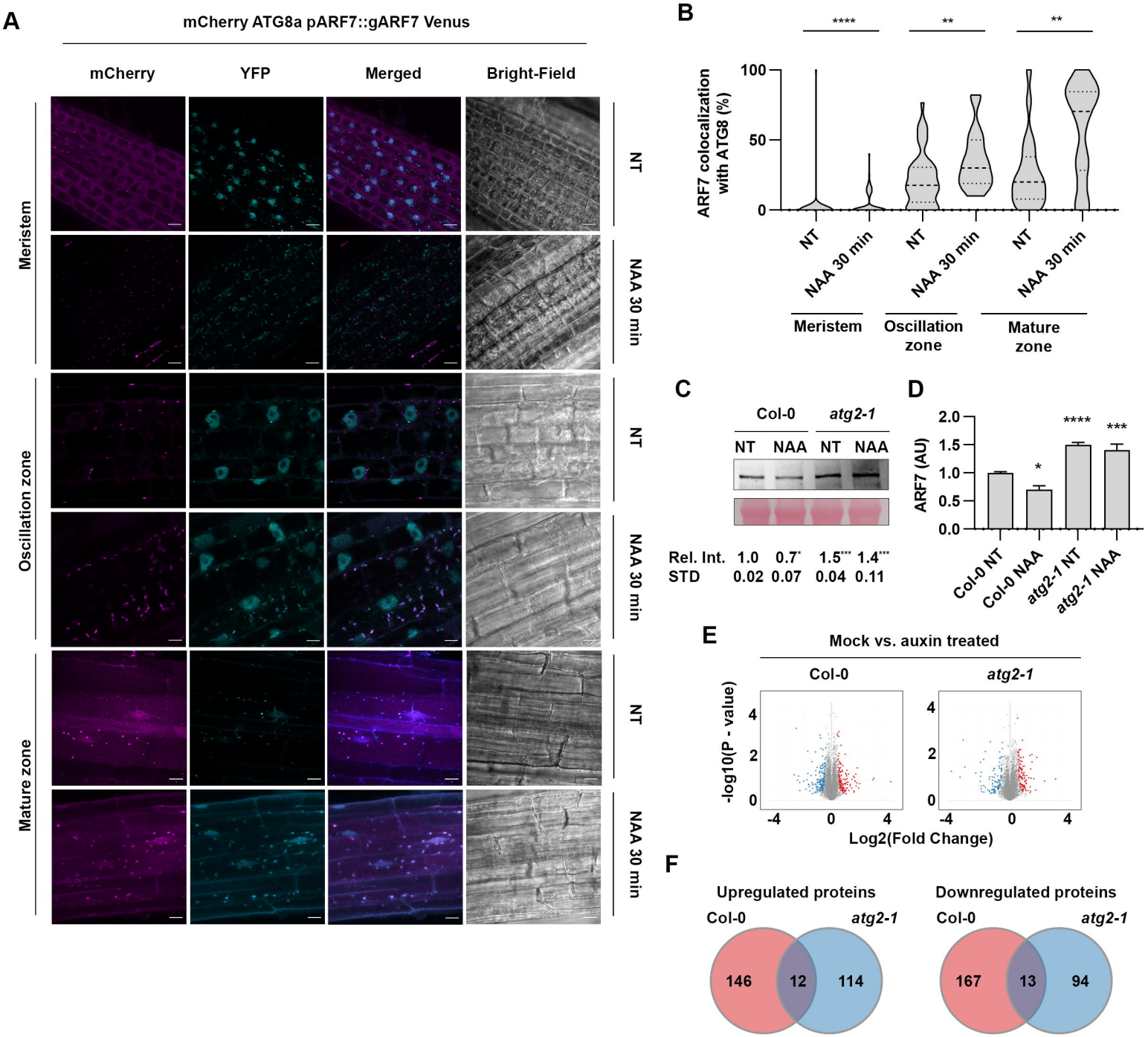
A
mCherry ATG8a pARF7::gARF7 Venus
mCherry
YFP
Merged
Bright-Field
Meristem
Oscillation zone
Mature zone
NT
NAA 30 min
B
****
**
**
ARF7 colocalization with ATG8 (%)
100
50
0
NT
NAA 30 min
Meristem
Oscillation zone
Mature zone
C
Col-0
atg2-1
NT
NAA
Rel. Int. 1.0 0.7* 1.5*** 1.4***
STD 0.02 0.07 0.04 0.11
D
ARF7 (AU)
2.0
1.5
1.0
0.5
0.0
*
****
***
Col-0 NT
Col-0 NAA
atg2-1 NT
atg2-1 NAA
E
Mock vs. auxin treated
Col-0
atg2-1
-log10(P - value)
Log2(Fold Change)
F
Upregulated proteins
Downregulated proteins
Col-0
atg2-1
146
12
114
167
13
94

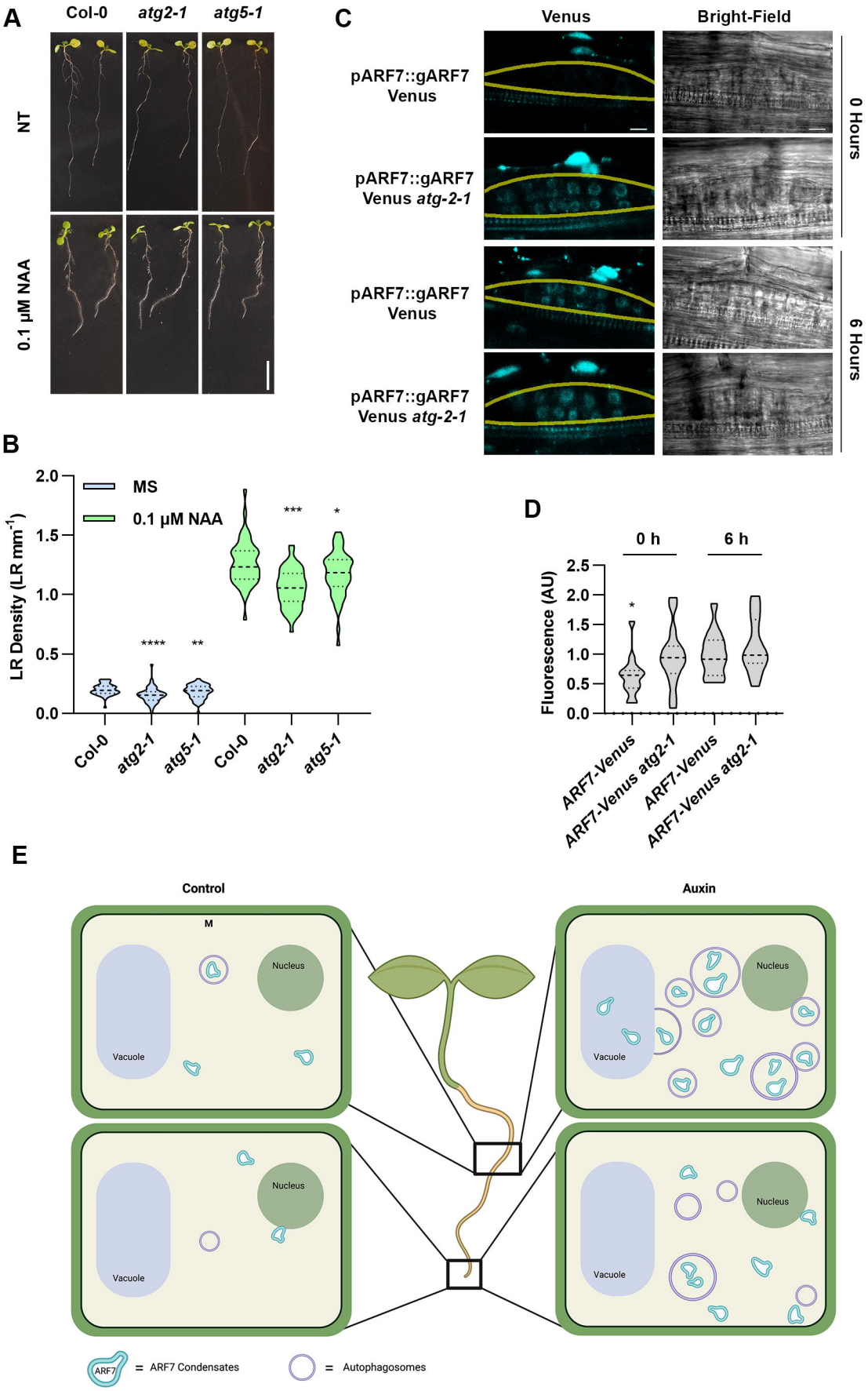
A
Col-0
atg2-1
atg5-1
NT
0.1 µM NAA
B
MS
0.1 µM NAA
LR Density (LR mm-1)
2.0
1.5
1.0
0.5
0.0
****
**
***
*
Col-0
atg2-1
atg5-1
Col-0
atg2-1
atg5-1
C
Venus
Bright-Field
pARF7::gARF7 Venus
pARF7::gARF7 Venus atg-2-1
pARF7::gARF7 Venus
pARF7::gARF7 Venus atg-2-1
0 Hours
6 Hours
D
0 h
6 h
Fluorescence (AU)
2.5
2.0
1.5
1.0
0.5
0.0
*
ARF7-Venus
ARF7-Venus atg2-1
ARF7-Venus
ARF7-Venus atg2-1
E
Control
Auxin
M
Nucleus
Vacuole
Nucleus
Vacuole
Nucleus
Vacuole
Nucleus
Vacuole
ARF7
= ARF7 Condensates
= Autophagosomes